AIMS Mathematics, 9(8): 21972–22001.
DOI: 10.3934/math.20241068
Received: 25 March 2024
Revised: 29 April 2024
Accepted: 13 May 2024
Published: 12 July 2024

http://www.aimspress.com/journal/Math

Research article

Threshold dynamics in a periodic epidemic model with imperfect quarantine, isolation and vaccination

Mahmoud A. Ibrahim[1,2,*]

[1] National Laboratory for Health Security, Bolyai Institute, University of Szeged, Aradi vértanúk tere 1., Szeged 6720, Hungary

[2] Department of Mathematics, Faculty of Science, Mansoura University, Mansoura 35516, Egypt

* **Correspondence:** Email: mibrahim@math.u-szeged.hu, mahmoud_ali@mans.edu.eg.

Abstract: A nonautonomous mathematical model was presented to explore the complex dynamics of disease spread over time, incorporating a time-periodic transmission parameter and imperfections in quarantine, isolation and vaccination strategies. Through a detailed examination of threshold dynamics, it was revealed that the global dynamics of disease transmission are influenced by the basic reproduction number ($\mathcal{R}_0$), a critical threshold that determines extinction, persistence, and the presence of periodic solutions. It was shown that the disease-free equilibrium is globally asymptotically stable if $\mathcal{R}_0 < 1$, while the disease persists if $\mathcal{R}_0 > 1$. To support and validate our analytical results, the basic reproduction number and the dynamics of the disease were estimated by fitting monthly data from two Asian countries, namely Saudi Arabia and Pakistan. Furthermore, a sensitivity analysis of the time-averaged reproduction number ($\langle\mathcal{R}_0\rangle$) of the associated time-varying model showed a significant sensitivity to key parameters such as infection rates, quarantine rate, vaccine coverage rate, and recovery rates, supported by numerical simulations. These simulations validated theoretical findings and explored the impact of seasonal contact rate, imperfect quarantine, isolation, imperfect vaccination, and other parameters on the dynamics of measles transmission. The results showed that increasing the rate of immunization, improving vaccine management, and raising public awareness can reduce the incidence of the epidemic. The study highlighted the importance of understanding these patterns to prevent future periodic epidemics.

Keywords: compartmental model; time-periodic transmission rates; basic reproduction number ($\mathcal{R}_0$); global dynamics; periodic solutions; sensitivity analysis
Mathematics Subject Classification: 34C23, 34C25, 34C60, 37N25, 92D25, 92D30

1. Introduction

In the relentless battle against infectious diseases, the development and refinement of mathematical models plays a crucial role in understanding the dynamics of epidemics and devising effective control strategies. The complex interplay of various factors, such as population heterogeneity, imperfect interventions, and periodic fluctuations, requires a comprehensive approach to model formulation. The dynamics of infectious diseases is influenced by the interaction between the pathogen and the host population, as well as the effectiveness of the control measures implemented [1]. In real-world scenarios, the implementation of quarantine, isolation, and vaccination strategies is often imperfect due to compliance issues, limited resources, and the emergence of new variants [2]. Understanding the impact of imperfect interventions on epidemic dynamics is crucial to designing robust public health strategies [3]. Imperfect quarantine and isolation can have an impact on the spread of infectious diseases. The use of quarantine and isolation as control measures can lead to the elimination of the disease if its level of effectiveness is sufficiently moderate [4]. However, the effectiveness of these measures may be influenced by other factors. For example, the level of transmission by isolated individuals in hospitals plays an important role in determining the impact of quarantine and isolation [5]. Furthermore, the combined use of quarantine and isolation with a vaccination strategy can further improve disease control and elimination [6]. It is important to note that the impact of quarantine and isolation can vary depending on the specific characteristics of the disease and the population studied.

The periodic nature of many infectious diseases, influenced by seasonal variations, environmental factors, or human behavior, adds an additional layer of complexity to the modeling framework [7–10]. Periodicity introduces threshold dynamics that govern the stability and persistence of epidemic cycles [11, 12]. Investigating the interaction between threshold dynamics and imperfect interventions is essential to understand disease transmission and control. In [13], the authors investigate the dynamical behavior of an SIRVS (susceptible - infected - recovered - vaccinated) epidemic model with time-dependent coefficients and give some new threshold conditions which determine whether or not the disease will go to extinction. In their work, [14] introduces a nonautonomous SIQR (susceptible - infected - quarantine - recovered) model that incorporates time-varying parameters and examines the criteria for eliminating or sustaining infection within this framework. The study defines critical thresholds for the autonomous, asymptotically autonomous and periodic scenarios, along with the general nonautonomous model featuring various forms of disease transmission.

Threshold dynamics in a periodic mathematical model with imperfect interventions have been studied in the context of various infectious diseases. The basic reproduction number ($\mathcal{R}_0$) is a key parameter that determines the persistence or extinction of the disease. If $\mathcal{R}_0$ is less than one, the disease will gradually disappear, while if $\mathcal{R}_0$ is greater than one, the disease will become endemic and persist [15–18]. The research by Safi et al. [19] examines a nonautonomous SEIRS (susceptible - exposed - infected - recovered) model that incorporates quarantine and isolation measures for a contagious disease. It shows that the disease-free state is globally asymptotically stable if the reproduction ratio is less than one, while the disease persists if the ratio exceeds one. The findings suggest that the introduction of periodicity into the autonomous quarantine/isolation model does not alter the threshold behavior of the system in terms of the elimination or persistence of the disease within the population. In [17], a mathematical model was established that includes a seasonal

transmission parameter and a double dose vaccination to examine how measles spreads over time. The basic reproduction number $\mathcal{R}_0$ was defined, and its utility as a threshold parameter for global dynamics and the existence of periodic solutions was demonstrated.

In this work, a nonautonomous mathematical model is developed to understand the spread of diseases over time, considering the complexities of periodic epidemic dynamics coupled with imperfections in quarantine, isolation, and vaccination strategies. Our model is based on previous work, specifically those presented in [5, 6, 17, 20, 21]. Through a comprehensive exploration of threshold dynamics, the global dynamics of disease transmission is governed by the basic reproduction number ($\mathcal{R}_0$). This number serves as a threshold value to determine the extinction or persistence of the disease, as well as the existence of periodic solutions. The following section introduces a comprehensive periodic model encompassing quarantine, isolation, and vaccination, revealing the presence of a disease-free equilibrium. Sections 3 to 6 are dedicated to derive the basic reproduction number ($\mathcal{R}_0$) for our model. These sections elucidate that, depending on its value, the disease-free equilibrium will either be globally stable or the disease will persist within the population. In Section 7, we integrate our model with the measles data from Saudi Arabia and Pakistan. Through this collaboration, we estimate various unknown parameters and determine the basic reproduction number. Furthermore, we illustrate the sensitivity of the parameters to the average reproduction number ($\langle\mathcal{R}_0\rangle$). Section 8 presents numerical simulations for both scenarios, reinforcing our theoretical findings. Subsequently, we performed numerical evaluations to examine the influence of seasonal contact rate, imperfect quarantine, isolation, imperfect vaccination, and other significant parameters on the transmission dynamics of measles. Section 9 contains our final discussion, summarizing the key findings and insights from the study.

2. Periodic model formulation

In this study, we consider the division of the total human population, indicated by $N(t)$, taking into account quarantine for exposed individuals, isolation for those with clinical symptoms of the disease, and vaccination. This partition was designed to analyze the dynamics of disease transmission and includes eight distinct compartments: susceptible ($S(t)$), individuals who have received the first dose of the vaccine ($V_1(t)$), those who have received the second dose of the vaccine ($V_2(t)$), exposed individuals who are infected but not yet show clinical symptoms of the disease ($E(t)$), infected individuals who are symptomatic ($I(t)$), quarantined individuals who are infected but do not display clinical symptoms of the disease ($Q(t)$), hospitalized individuals ($H(t)$) and recovered individuals ($R(t)$).

Quarantine in general involves the isolation of susceptible individuals suspected of exposure to a disease, but in this work, quarantine refers to the removal of newly-infected individuals from contact with the general population [19, 22]. This is because quarantine of susceptible individuals is unlikely to significantly impact disease dynamics for large total population sizes, as it only involves newly-infected individuals detected through contact tracing or random testing. Those who remain susceptible at the end of the quarantine period are not included in the Q class [19, 22].

Displayed in Figure 1 is the transition of individuals among compartments, while the model equations are expressed as follows:

$$
\begin{aligned}
\frac{dS(t)}{dt} &= \Lambda - \lambda(t)S(t) - (\theta + \mu)S(t),\\
\frac{dV_1(t)}{dt} &= \theta S(t) - (1-\alpha_1)\lambda(t)V_1(t) - (\sigma_1 + \mu)V_1(t),\\
\frac{dV_2(t)}{dt} &= \sigma_1 V_1(t) - (1-\alpha_2)\lambda(t)V_2(t) - (\sigma_2 + \mu)V_2(t),\\
\frac{dE(t)}{dt} &= \lambda(t)(S(t) + (1-\alpha_1)V_1(t) + (1-\alpha_2)V_2(t)) - (\nu_1 + \nu_2 + \mu)E(t),\\
\frac{dI(t)}{dt} &= \nu_1 E(t) - \gamma_1 I(t) - \kappa_1 I(t) - (\delta_1 + \mu)I(t),\\
\frac{dQ(t)}{dt} &= \nu_2 E(t) - \gamma_2 Q(t) - \kappa_2 Q(t) - \mu Q(t),\\
\frac{dH(t)}{dt} &= \kappa_1 I(t) + \kappa_2 Q(t) - \gamma_3 H(t) - (\delta_2 + \mu)H(t),\\
\frac{dR(t)}{dt} &= \gamma_1 I(t) + \gamma_2 Q(t) + \gamma_3 H(t) + \sigma_2 V_2(t) - \mu R(t),
\end{aligned}
\tag{2.1}
$$

where

$$
\lambda(t) = \beta(t)\frac{\tau_e E(t) + I(t) + \tau(\varepsilon_1 Q(t) + \varepsilon_2 H(t))}{N(t) - (1-\varepsilon_1)Q(t) - (1-\varepsilon_2)H(t)},
$$

denotes the time-dependent infection rate and $N(t) - (1-\varepsilon_1)Q(t) - (1-\varepsilon_2)H(t) = S(t) + V_1(t) + V_2(t) + I(t) + \varepsilon_1 Q(t) + \varepsilon_2 H(t) + R(t)$ is the total actively-mixing population.

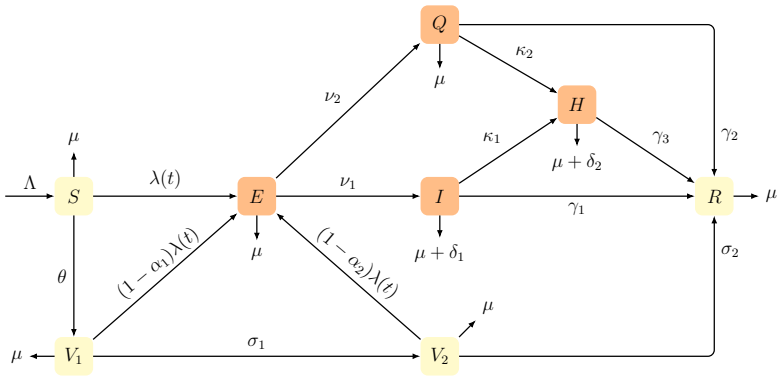

Figure 1. Schematic diagram of disease transmission in a population.

In the system (2.1), we assume that the effective contact rate $\beta(t)$ is a continuous, positive ω-periodic function. The human recruitment rate and the natural death rate are denoted by Λ and μ, respectively. Susceptible individuals who have received the first dose of the vaccine transition to the vaccinated compartment V_1 at a rate of θ. Because the first dose of the disease vaccine is not very effective, people who have had a single dose can contract the disease by coming into contact with infected people at a rate of $(1-\alpha_1)\lambda(t)$. On the other hand, most people fall into the category of people who have received two doses at a rate of σ_1, as explained in [17, 20, 23]. Unlike [17, 20, 23], and in agreement with [24], we assume that the second dose of the vaccine is ineffective in preventing the disease. Individuals with two doses can contract the disease by contact with infected individuals at a rate of $(1-\alpha_2)\lambda(t)$, while

the majority of the population transitions to the recovery class at a rate of σ_2. It is important to note that $\alpha_1 = 0$ or $\alpha_2 = 0$ indicates a vaccine that offers no protection at all, while $\alpha_1 = 1$ or $\alpha_2 = 1$ represents a perfect vaccine, with $0 < \alpha_1, \alpha_2 < 1$. Based on the insights of [19], it is important to note that, in the context of this study, the quarantine process usually involves isolating susceptible individuals suspected of exposure to the disease. Specifically, the quarantine class (Q) comprises newly infected (asymptomatic) individuals, with detection usually carried out through contact tracing or random tests. In this study, quarantine specifically refers to the separation of newly infected individuals from the general population. Consequently, individuals who remain susceptible at the end of the quarantine period are not considered to be part of the Q class. The parameters ε_1 and ε_2, both of which range from 0 to 1, act as modifiers to measure the effectiveness of quarantine and isolation. Perfection is achieved when $\varepsilon_1 = 0 = \varepsilon_2$, ensuring that individuals in these categories avoid contact with the general public, thus preventing the transmission of infection. Leaky quarantine is represented by $0 < \varepsilon_1, \varepsilon_2 < 1$. On the contrary, when $\varepsilon_1 = 1 = \varepsilon_2$, people in quarantine and isolation are as likely as any other member of the population to interact with the general public. We provide a complete description of the model parameters, which is presented in Table 1.

Table 1. Description of parameters for model (2.1).

Parameters	Description
Λ	Recruitment rate of susceptible humans
μ	Natural death rate
$\beta(t)$	Periodic transmission rate of symptomatic infection
τ_e	Relative transmissibility of exposed to infected
τ	Relative transmissibility of quarantined and hospitalized to infected
α_1, α_2	Modification parameters for vaccine efficacy
ε_1, ε_2	Modification parameters for the efficacy of quarantine and isolation
θ	Coverage rate of vaccine for entire population
σ_1	Rate of vaccination with second dose
σ_2	Progression rate from V_2 to R
ν_1	Progression rate from exposed to infectious class
ν_2	Quarantine rate for exposed individuals
κ_1, κ_2	Hospitalization rate for infectious and quarantined individuals
γ_1, γ_2, γ_2	Recovery rate for infectious, quarantined, and hospitalized individuals
δ_1, δ_2	Disease-induced death rate for infectious and hospitalized individuals

It is evident that any solution to the system (2.1) that begins with nonnegative initial values will also be nonnegative. Therefore, we will first examine the bounds of the solution of this system.

Define

$$\begin{aligned} X &= \left\{(S, V_1, V_2, E, I, Q, H, R) \in \mathbb{R}_+^8 : S + V_1 + V_2 + E + I + Q + H + R \leq N\right\}, \\ X(0) &= (S(0), V_1(0), V_2(0), E(0), I(0), Q(0), H(0), R(0)) \in \mathbb{R}_+^8, \end{aligned} \tag{2.2}$$

and let Ψ be defined as the set

$$\Psi := \left\{(S, V_1, V_2, E, I, Q, H, R) \in X : S + V_1 + V_2 + E + I + Q + H + R = N \leq \frac{\Lambda}{\mu}\right\}.$$

Under this definition, we introduce the following lemma.

Lemma 1. *The solution to System* (2.1) *is both unique and bounded, given the initial value* $X(0) \in X$ *defined in* (2.2)*. Moreover, the set* Ψ *is compact, positively invariant, and attracts all positive orbits in* X*.*

Proof. Consider $X_1 = (S, V_1, V_2, E, I, Q, H, N)$. Building upon references [19,25,26], we introduce the functions $g_1, g_2, g_3 \in (\mathbb{R}^8_+, \mathbb{R}_+)$ defined as follows:

$$\begin{aligned}
g_1(X_1) &= \begin{cases} 0, & \text{if } X_1 = (0,0,0,0,0,0,0,0), \\ \frac{I+\tau_e E+\tau(\varepsilon_1 Q+\varepsilon_2 H)}{N-(1-\varepsilon_1)Q-(1-\varepsilon_2)H} S, & \text{otherwise.} \end{cases} \\
g_2(X_1) &= \begin{cases} 0, & \text{if } X_1 = (0,0,0,0,0,0,0,0), \\ \frac{I+\tau_e E+\tau(\varepsilon_1 Q+\varepsilon_2 H)}{N-(1-\varepsilon_1)Q-(1-\varepsilon_2)H} V_1, & \text{otherwise.} \end{cases} \\
g_3(X_1) &= \begin{cases} 0, & \text{if } X_1 = (0,0,0,0,0,0,0,0), \\ \frac{I+\tau_e E+\tau(\varepsilon_1 Q+\varepsilon_2 H)}{N-(1-\varepsilon_1)Q-(1-\varepsilon_2)H} V_2, & \text{otherwise.} \end{cases}
\end{aligned} \tag{2.3}$$

Through a change of variable where $N = S + V_1 + V_2 + E + I + Q + H + R$ and from (2.3), system (2.1) can be reformulated as follows:

$$\begin{aligned}
\frac{\mathrm{d}S(t)}{\mathrm{d}t} &= \Lambda - \beta(t) g_1(X_1) - (\theta + \mu) S(t), \\
\frac{\mathrm{d}V_1(t)}{\mathrm{d}t} &= \theta S(t) - (1-\alpha_1)\beta(t) g_2(X_1) - (\sigma_1 + \mu) V_1(t), \\
\frac{\mathrm{d}V_2(t)}{\mathrm{d}t} &= \sigma_1 V_1(t) - (1-\alpha_2)\beta(t) g_3(X_1) - (\sigma_2 + \mu) V_2(t), \\
\frac{\mathrm{d}E(t)}{\mathrm{d}t} &= \beta(t) g_1(X_1) + (1-\alpha_1)\beta(t) g_2(X_1) + (1-\alpha_2)\beta(t) g_3(X_1) - (\nu_1 + \nu_2 + \mu) E(t), \\
\frac{\mathrm{d}I(t)}{\mathrm{d}t} &= \nu_1 E(t) - \gamma_1 I(t) - \kappa_1 I(t) - (\delta_1 + \mu) I(t), \\
\frac{\mathrm{d}Q(t)}{\mathrm{d}t} &= \nu_2 E(t) - \gamma_2 Q(t) - \kappa_2 Q(t) - \mu Q(t), \\
\frac{\mathrm{d}H(t)}{\mathrm{d}t} &= \kappa_1 I(t) + \kappa_2 Q(t) - \gamma_3 H(t) - (\delta_2 + \mu) H(t), \\
\frac{\mathrm{d}N(t)}{\mathrm{d}t} &= \Lambda - \delta_1 I(t) - \delta_2 H(t) - \mu N(t).
\end{aligned} \tag{2.4}$$

It is evident that $g_1(X_1)$, $g_2(X_1)$, and $g_3(X_1)$ are continuous and globally Lipschitz in $\mathbb{R}^8_+$. Applying Theorem 5.2.1 from [27] allows us to establish that, for any $(S(0), V_1(0), V_2(0), E(0), I(0), Q(0), H(0), N(0)) \in \mathbb{R}^8_+$, the system (2.4) possesses a unique local nonnegative solution $(S, V_1, V_2, E, I, Q, H, N)$.

From the total human population $N(t)$ with a positive initial condition $X(0) \in \mathbb{R}^8_+$, we have the equation

$$\frac{\mathrm{d}N(t)}{\mathrm{d}t} = \Lambda - \delta_1 I(t) - \delta_2 H(t) - \mu N(t) \leq \Lambda - \mu N(t),$$

indicating that the associated linear differential equation,

$$\frac{\mathrm{d}N(t)}{\mathrm{d}t} = \Lambda - \mu N(t),$$

has a unique equilibrium $N^* = \frac{\Lambda}{\mu}$ in $\mathbb{R}_+$. Hence, as $t \to \infty$, the difference $|N(t) - N^*|$ tends to zero and N^* becomes globally attractive in $\mathbb{R}_+$. Additionally, employing the comparison theorem [28] confirms that $N(t)$ remains bounded. Consequently, the solution of the system (2.1) exists globally over the interval $[0, \infty)$. □

The equilibrium without the presence of the disease, known as the disease-free equilibrium in (2.1), can be determined by solving the system below:

$$\begin{aligned} 0 &= \Lambda - (\theta + \mu)S^*, \\ 0 &= \theta S^* - (\sigma_1 + \mu)V_1^*, \\ 0 &= \sigma_1 V_1^* - (\sigma_2 + \mu)V_2^*, \\ 0 &= \sigma_2 V_2^* - \mu R^*. \end{aligned} \tag{2.5}$$

Clearly, the solution to (2.5) is the unique disease-free equilibrium of system (2.1), as given by:

$$\begin{aligned} \mathcal{D}_0 &= (S^*, V_1^*, V_2^*, 0, 0, 0, 0, R^*) \\ &= \left(S^*, \frac{\theta}{\sigma_1 + \mu}S^*, \frac{\sigma_1\theta}{(\sigma_1 + \mu)(\sigma_2 + \mu)}S^*, 0, 0, 0, 0, \frac{\sigma_1\sigma_2\theta}{\mu(\sigma_1 + \mu)(\sigma_2 + \mu)}S^*\right), \end{aligned}$$

where $S^* = \dfrac{\Lambda}{\theta + \mu}$.

3. Basic reproduction number

For periodic epidemic compartmental models, Bacaër and Guernaou [29] provided a definition of $\mathcal{R}_0$ as the spectral radius of an integral operator acting on the space of continuous periodic functions. Later, Wang and Zhao [11] characterized $\mathcal{R}_0$ for such models and proved that it serves as a threshold parameter regarding the local stability properties of the disease-free periodic solution. Rebelo et al. [12] studied persistence in epidemiological models in a seasonal environment. Bacaër and Ait Dads [30] gave a more biological explanation of $\mathcal{R}_0$ for compartmental epidemic models with periodic parameters. Therefore, the global dynamics of the system is characterized by the basic reproduction number ($\mathcal{R}_0$) of periodic compartmental models.

Within this section, we employ the methodology introduced in [11, 12, 31] to determine the basic reproduction number ($\mathcal{R}_0$) for the system (2.1). Define the vector $\mathcal{H} = (E, I, Q, H, S, V_1, V_2, R)^T$, where E, I, Q, and H correspond to the infected classes, and S, V_1, V_2, and R denote the uninfected classes with

$$\mathcal{F}(t, \mathcal{H}(t)) = \begin{bmatrix} \lambda(t)(S(t) + (1 - \alpha_1)V_1(t) + (1 - \alpha_2)V_2(t)) \\ 0 \\ 0 \\ 0 \\ 0 \\ 0 \\ 0 \\ 0 \end{bmatrix},$$

$$\mathcal{V}^{-}(t,\mathcal{H}(t)) = \begin{bmatrix} (\nu_1+\nu_2+\mu)E(t) \\ \gamma_1 I(t)+\kappa_1 I(t)+(\delta_1+\mu)I(t) \\ \kappa_2 Q(t)+\gamma_2 Q(t)+\mu Q(t) \\ \gamma_3 H(t)+(\delta_2+\mu)H(t) \\ \lambda(t)S(t)+(\theta+\mu)S(t) \\ ((1-\alpha_1)\lambda(t)+\sigma_1+\mu)V_1(t) \\ ((1-\alpha_2)\lambda(t)+\sigma_2+\mu)V_2(t) \\ \mu R(t) \end{bmatrix}, \quad \mathcal{V}^{+}(t,\mathcal{H}(t)) = \begin{bmatrix} 0 \\ \nu_1 E(t) \\ \nu_2 E(t) \\ \kappa_1 I(t)+\kappa_2 Q(t) \\ \Lambda \\ \theta S(t) \\ \sigma_1 V_1(t) \\ \gamma_1 I(t)+\gamma_2 Q(t)+\gamma_3 H(t)+\sigma_2 V_2(t) \end{bmatrix}.$$

The nonautonomous equation presented below,

$$\mathcal{H}'(t) = \mathcal{F}(t,\mathcal{H}(t)) - \mathcal{V}(t,\mathcal{H}(t)) = \mathcal{F}(t,\mathcal{H}(t)) + \mathcal{V}^{+}(t,\mathcal{H}(t)) - \mathcal{V}^{-}(t,\mathcal{H}(t)), \tag{3.1}$$

is equivalent to System (2.1). The disease-free equilibrium for (3.1) is $\mathcal{H}^* = \left(0,0,0,0,S^*,V_1^*,V_2^*,R^*\right)$. To start the analysis, we verify that the model (2.1) satisfies the conditions (A1)–(A7) outlined in [11]. Subsequently, we determine the matrix functions 4×4, $F(t) = (\frac{\partial \mathcal{F}_i(t,\mathcal{H}^*)}{\partial \mathcal{H}_j})_{1\leqslant i,j\leqslant 4}$, and $V(t) = (\frac{\partial \mathcal{V}_i(t,\mathcal{H}^*)}{\partial \mathcal{H}_j})_{1\leqslant i,j\leqslant 4}$ in the following manner:

$$F(t) = \begin{bmatrix} \tau_e\beta(t)L^* & \beta(t)L^* & \tau\epsilon_1\beta(t)L^* & \tau\epsilon_2\beta(t)L^* \\ 0 & 0 & 0 & 0 \\ 0 & 0 & 0 & 0 \\ 0 & 0 & 0 & 0 \end{bmatrix},$$

and

$$V(t) = \begin{bmatrix} \nu_1+\nu_2+\mu & 0 & 0 & 0 \\ -\nu_1 & \gamma_1+\kappa_1+\delta_1+\mu & 0 & 0 \\ -\nu_2 & 0 & \gamma_2+\kappa_2+\mu & 0 \\ 0 & -\kappa_1 & -\kappa_2 & \gamma_3+\delta_2+\mu \end{bmatrix},$$

where $L^* = \frac{S^*+(1-\alpha_1)V_1^*+(1-\alpha_2)V_2^*}{N^*}$. Conditions (A1) through (A6) provided in [11] are easily verified, and the disease-free subspace $\mathcal{H}^*$ is linearly asymptotically stable at $\mathcal{H}_s = (0,0,0,0,S,V_1,V_2,R) \in \mathbb{R}_+^8$.

Consider $\mathbf{G}(x,y)$ as a matrix solution to the initial value problem presented below, where $x \geqslant y$:

$$\frac{\mathrm{d}\mathbf{G}(x,y)}{\mathrm{d}x} = -V(x)\mathbf{G}(x,y), \quad \mathbf{G}(y,y) = I, \quad \forall x \geqslant y, \tag{3.2}$$

where I is the 4×4 identity matrix. Thus, $\mathbf{G}(x,y)$ can easily be calculated as

$$\mathbf{G}(x,y) = \begin{bmatrix} e^{-(\nu_1+\nu_2+\mu)(x-y)} & 0 & 0 & 0 \\ -\nu_1\frac{e^{-(\nu_1+\nu_2+\mu)(x-y)}-e^{-(\gamma_1+\kappa_1+\delta_1+\mu)(x-y)}}{(\nu_1+\nu_2-\gamma_1-\kappa_1-\delta_1)} & e^{-(\gamma_1+\kappa_1+\delta_1+\mu)(x-y)} & 0 & 0 \\ -\nu_2\frac{e^{-(\nu_1+\nu_2+\mu)(x-y)}-e^{-(\gamma_2+\kappa_2+\mu)(x-y)}}{(\nu_1+\nu_2-\gamma_2+\kappa_2)} & 0 & e^{-(\gamma_2+\kappa_2+\mu)(x-y)} & 0 \\ G_{31}(x,y) & -\kappa_1 G_{32}(x,y) & -\kappa_2 G_{33}(x,y) & e^{-(\gamma_3+\delta_2+\mu)(x-y)} \end{bmatrix},$$

where

$$G_{31}(x,y) = \frac{((\gamma_1+\kappa_1+\delta_1-\gamma_3-\delta_2)\kappa_2\nu_2+(\nu_1+\nu_2-\gamma_2-\kappa_2)\kappa_1\nu_1)}{(\nu_1+\nu_2-\gamma_1-\kappa_1-\delta_1)(\nu_1+\nu_2-\gamma_2-\kappa_2)(\nu_1+\nu_2-\gamma_3-\delta_2)}e^{-(\nu_1+\nu_2+\mu)(x-y)}$$

$$+\frac{((\nu_1+\nu_2-\gamma_1-\kappa_1-\delta_1)\kappa_2\nu_2+(\gamma_2+\kappa_2-\gamma_3-\delta_2)\kappa_1\nu_1)}{(\nu_1+\nu_2-\gamma_3-\delta_2)(\gamma_1+\kappa_1+\delta_1-\gamma_3-\delta_2)(\gamma_2+\kappa_2-\gamma_3-\delta_2)}e^{-(\gamma_3+\delta_2+\mu)(x-y)}$$
$$-\frac{\kappa_1\nu_1}{(\nu_1+\nu_2-\gamma_1-\kappa_1-\delta_1)(\gamma_1+\kappa_1+\delta_1-\gamma_3-\delta_2)}e^{-(\gamma_1+\kappa_1+\delta_1+\mu)(x-y)}$$
$$-\frac{\kappa_2\nu_2}{(\nu_1+\nu_2-\gamma_2-\kappa_2)(\gamma_2+\kappa_2-\gamma_3-\delta_2)}e^{-(\gamma_2+\kappa_2+\mu)(x-y)},$$

$$G_{32}(x,y)=\frac{e^{-(\gamma_1+\kappa_1+\delta_1+\mu)(x-y)}-e^{-(\gamma_3+\delta_2+\mu)(x-y)}}{\gamma_1+\kappa_1+\delta_1-\gamma_3-\delta_2},\qquad G_{33}(x,y)=\frac{e^{-(\gamma_2+\kappa_2+\mu)(x-y)}-e^{-(\gamma_3+\delta_2+\mu)(x-y)}}{\gamma_2+\kappa_2-\gamma_3-\delta_2}.$$

Therefore, the requirement (A7) described in [11] is met, as the matrix $\Psi_{-V}(x)$ of (3.2) for $x \geqslant 0$ is equivalent to $\mathbf{G}(x,0)$. Let $\mathcal{B}_\omega$ represent the ordered Banach space of ω-periodic functions from $\mathbb{R}$ to $\mathbb{R}^4$, equipped with the usual maximum norm $\|\cdot\|_\infty$. Additionally, define $\mathcal{B}_\omega^+ := \{\phi \in \mathcal{B}_\omega : \phi(t) \geqslant 0,\ \forall t \in \mathbb{R}\}$ as the positive cone.

Define the linear next-generation operator (NGO) $\mathcal{K}$, responsible for subsequent infections, which maps $\mathcal{B}_\omega$ to $\mathcal{B}_\omega$ as given below:

$$(\mathcal{K}\phi)(x)=\int_0^\infty \mathbf{G}(x,x-r)F(x-r)\phi(x-r)dr,\quad \forall\ \phi\in\mathcal{B}_\omega,\ x\in\mathbb{R}.$$

The basic reproduction number $\mathcal{R}_0$ for the model (2.1) can be computed as the spectral radius of $\mathcal{K}$, denoted as $\mathcal{R}_0 := \rho(\mathcal{K})$.

In order to calculate an approximate numerical value for $\mathcal{R}_0$, as described in [11], we define $\Psi_{\frac{F}{\lambda}-V}(t,\lambda)$ as the fundamental matrix of the linear ω-periodic equation

$$\mathbf{x}'=\left[\frac{F(t)}{\lambda}-V(t)\right]\mathbf{x},\quad \forall t\in\mathbb{R}, \tag{3.3}$$

where λ is a parameter in the interval $(0,\infty)$. Additionally, without losing generality, we make the assumption that $\Psi_{\frac{F}{\lambda}-V}(0,\lambda)$ is equivalent to the identity matrix I. It is crucial to keep in mind that $\Psi_{\frac{F}{\lambda}-V}(\omega,\lambda)$ represents the monodromy matrix of the linear ω-periodic system (3.3).

Theorem 2 ([11, Theorem 2.1])**.** *The following assertions are valid.*

(i) If $\rho(\Psi_{\frac{F}{\lambda}-V}(\omega,\lambda))=1$ has a positive solution λ_0, then λ_0 is an eigenvalue of operator $\mathcal{K}$ and, hence, $\mathcal{R}_0>0$.

(ii) If $\mathcal{R}_0>0$, then $\lambda_0=\mathcal{R}_0$ is a unique solution of $\rho(\Psi_{\frac{F}{\lambda}-V}(\omega,\lambda))=1$.

(iii) $\mathcal{R}_0=0$ if and only if $\rho(\Psi_{\frac{F}{\lambda}-V}(\omega,\lambda))<1$ for all $\lambda>0$.

More details about the numerical method used to compute the basic reproduction number $\mathcal{R}_0$ (the spectral radius of the NGO $\mathcal{K}$) can be found in [32, 33].

4. Stability analysis of the disease-free equilibrium ($\mathcal{D}_0$) of system (2.1)

In this section, our objective is to demonstrate the local and global stability of $\mathcal{D}_0$ and establish that the disease undergoes extinction when $\mathcal{R}_0<1$.

Consider $\Psi_{F-V}(t)$ as a fundamental matrix of the linear ω-periodic system $\mathbf{x}' = [F(t) - V(t)]\mathbf{x}$. Additionally, and without loss of generality, assume that $\Psi_{F-V}(0) = I$, representing the identity matrix. It is important to note that $\Psi_{F-V}(\omega)$ is the monodromy matrix of the linear ω-periodic system mentioned above. Now, we recall the following Theorem 2.2 from [11] regarding the local stability of the disease-free equilibrium $\mathcal{D}_0$.

Theorem 3 ([11], Theorem 2.2)**.** *The following statements are valid:*

(i) $\rho(\Psi_{F-V}(\omega)) < 1(> 1) \iff \mathcal{R}_0 < 1(> 1)$*;*

(ii) $\rho(\Psi_{F-V}(\omega)) = 1 \iff \mathcal{R}_0 = 1$.

Building on the preceding discussion, the subsequent theorem delves into the local stability of the disease-free equilibrium $\mathcal{D}_0$ of (2.1).

Theorem 4. *The disease-free equilibrium $\mathcal{D}_0$ is locally asymptotically stable if $\mathcal{R}_0 < 1$ and unstable if $\mathcal{R}_0 > 1$.*

Proof. Consider the Jacobian matrix of (2.1) calculated at $\mathcal{D}_0$, represented as

$$J(t) = \begin{bmatrix} F(t) - V(t) & 0 \\ \mathcal{A}_1(t) & \mathcal{A}_2 \end{bmatrix},$$

where

$$\mathcal{A}_1(t) = \begin{bmatrix} \tau_e\beta(t)\frac{S^*}{N^*} & \beta(t)\frac{S^*}{N^*} & \tau\beta(t)\frac{S^*}{N^*} & \tau\beta(t)\frac{S^*}{N^*} \\ \tau_e\beta(t)\frac{(1-\alpha_1)V_1^*}{N^*} & \beta(t)\frac{(1-\alpha_1)V_1^*}{N^*} & \tau\beta(t)\frac{(1-\alpha_1)V_1^*}{N^*} & \tau\beta(t)\frac{(1-\alpha_1)V_1^*}{N^*} \\ \tau_e\beta(t)\frac{(1-\alpha_2)V_2^*}{N^*} & \beta(t)\frac{(1-\alpha_2)V_2^*}{N^*} & \tau\beta(t)\frac{(1-\alpha_2)V_2^*}{N^*} & \tau\beta(t)\frac{(1-\alpha_2)V_2^*}{N^*} \\ 0 & \gamma_1 & \gamma_2 & \gamma_3 \end{bmatrix},$$

and

$$\mathcal{A}_2 = \begin{bmatrix} -\theta - \mu & 0 & 0 & 0 \\ \theta & -\sigma_1 - \mu & 0 & 0 \\ 0 & \sigma_1 & -\sigma_2 - \mu & 0 \\ 0 & 0 & \sigma_2 & -\mu \end{bmatrix}.$$

Referring to [34], the local asymptotic stability of $\mathcal{D}_0$ is contingent on two conditions: $\rho(\Psi_{\mathcal{A}_2}(\omega)) < 1$ and $\rho(\Psi_{F-V}(\omega)) < 1$. Here, $\mathcal{A}_2$ is a constant matrix with negative eigenvalues $-(\theta + \mu) < 0$, $-(\sigma_1 + \mu) < 0$, $-(\sigma_2 + \mu) < 0$, and $-\mu < 0$, so $\rho(\Psi_{\mathcal{A}_2}) < 1$. The stability of $\mathcal{D}_0$ is ultimately determined by $\rho(\Psi_{F-V}(\omega))$. Therefore, $\mathcal{D}_0$ is locally asymptotically stable if $\rho(\Psi_{F-V}(\omega)) < 1$ and unstable if $\rho(\Psi_{F-V}(\omega)) > 1$. This completes the proof using Theorem 3. □

Theorem 5. *If $\mathcal{R}_0 < 1$, then the disease-free equilibrium $\mathcal{D}_0$ of* (2.1) *is globally asymptotically stable.*

Proof. Extending our analysis to local stability in Theorem 4, if $\mathcal{R}_0 < 1$, the disease-free equilibrium $\mathcal{H}^*$ is proven to be locally asymptotically stable. However, to establish global attractiveness, it is essential to confirm the fulfillment of requirements (A1) through (A7) as outlined in [12], discussed in Section 3. Furthermore, note that $\mathcal{H}^* = \left(0, 0, 0, 0, S^*, V_1^*, V_2^*, R^*\right)$ stands as the unique equilibrium of (3.1) within the set of disease-free states $\mathcal{H}_s$.

The first three equations of (2.1) yield the following system:

$$\begin{aligned}
S'(t) &= \Lambda - \lambda(t)S(t) - (\theta + \mu)S(t),\\
V_1'(t) &= \theta S(t) - (1-\alpha_1)\lambda(t)V_1(t) - (\sigma_1 + \mu)V_1(t),\\
V_2'(t) &= \sigma_1 V_1(t) - (1-\alpha_2)\lambda(t) - (\sigma_2 + \mu)V_2(t).
\end{aligned}$$

Considering the nonnegativity constraints $E(t) \geq 0$, $I(t) \geq 0$, $Q(t) \geq 0$, and $H(t) \geq 0$ established in Lemma 1, we can deduce the following inequalities:

$$\begin{aligned}
S'(t) &\leq \Lambda - (\theta + \mu)S(t),\\
V_1'(t) &\leq \theta S(t) - (\sigma_1 + \mu)V_1(t),\\
V_2'(t) &\leq \sigma_1 V_1(t) - (\sigma_2 + \mu)V_2(t).
\end{aligned}$$

These inequalities imply:

$$\begin{aligned}
\limsup_{t\to\infty} S(t) &\leq \frac{\Lambda}{\theta + \mu} = S^*,\\
\limsup_{t\to\infty} V_1(t) &\leq \frac{\theta S^*}{\sigma_1 + \mu} = \frac{\theta\Lambda}{(\theta + \mu)(\sigma_1 + \mu)} = V_1^*,\\
\limsup_{t\to\infty} V_2(t) &\leq \frac{\sigma_1 V_1^*}{\sigma_2 + \mu} = \frac{\sigma_1\theta\Lambda}{(\theta + \mu)(\sigma_1 + \mu)(\sigma_2 + \mu)} = V_2^*.
\end{aligned}$$

Consequently, for any arbitrary positive m, there exists $t(m) > 0$ such that $S(t) \leq S^* + m$, $V_1(t) \leq V_1^* + m$, and $V_2(t) \leq V_2^* + m$ for all $t > t(m)$.

We define $q(m) := \min\{\frac{S^* + (1-\alpha_1)V_1^* + (1-\alpha_2)V_2^*}{S^* + m + (1-\alpha_1)(V_1^* + m) + (1-\alpha_2)(V_2^* + m)}\}$. From the system in (2.1), for $t > t(m)$, the following inequalities can be derived:

$$\begin{aligned}
E'(t) &\leq \beta(t)(\tau_e E(t) + I(t) + \tau(\varepsilon_1 Q(t) + \varepsilon_2 H(t)))\frac{1}{q(m)} - (\nu_1 + \nu_2 + \mu)E(t),\\
I'(t) &\leq \nu_1 E(t) - \gamma_1 I(t) - \kappa_1 I(t) - (\delta_1 + \mu)I(t),\\
Q'(t) &\leq \nu_2 E(t) - \kappa_2 Q(t) - \gamma_2 Q(t) - \mu Q(t),\\
H'(t) &\leq \kappa_1 I(t) + \kappa_2 Q(t) - \gamma_3 H(t) - (\delta_2 + \mu)H(t),
\end{aligned} \tag{4.1}$$

and system (4.1) can be reformulated as

$$\mathcal{Y}'(t) \leqslant (\frac{F(t)}{q(m)} - V(t))\mathcal{Y}(t), \quad \forall t \geqslant t(m), \tag{4.2}$$

with $\mathcal{Y}(t) = (E(t), I(t), Q(t), H(t))$. In the limit as t approaches infinity, $\mathcal{Y}(t)$ tends to zero, signifying the eventual extinction of the disease. Using ([12], Theorem 2), it follows that $\mathcal{H}^*$ achieves global asymptotic stability (GAS) due to its GAS behavior within the disease-free subspace $\mathcal{H}_s$. □

5. Persistence of the infective compartments

In this subsection, we employ the methodology introduced by [12] to showcase the persistence of infective compartments within the system (2.1) when $\mathcal{R}_0 > 1$.

Theorem 6. *If $\mathcal{R}_0 > 1$, the dynamical system described by* (2.1) *displays persistent behavior regarding the variables E, I, Q, and H.*

Proof. Given the persistence of the sum $E + I + Q$, we can establish the persistence of each infectious variable E, I, and Q, ultimately resulting in the persistence of variable H. Let ε be a positive value such that $\liminf_{t\to+\infty}(E + I + Q) \geqslant m$. Consequently, for large values of t, it can be deduced that $E \geqslant \frac{m}{3} - I - Q$. Obtaining expressions for I' and Q' from the equations in (2.1), we derive the following inequalities:

$$\begin{aligned} I'(t) &\geq \nu_1\frac{m}{3} - \nu_1 Q(t) - (\nu_1 + \gamma_1 + \kappa_1 + \delta_1 + \mu)I(t), \\ Q'(t) &\geq \nu_2\frac{m}{3} - \nu_2 I(t) - (\nu_2 + \kappa_2 + \gamma_2 + \mu)Q(t). \end{aligned}$$

Consequently, we can infer that

$$\begin{aligned} I(t) &\geq \frac{\nu_1 m}{3(\nu_1 + \gamma_1 + \kappa_1 + \delta_1 + \mu)} =: \kappa_i(m), \\ Q(t) &\geq \frac{\nu_2 m}{3(\nu_2 + \kappa_2 + \gamma_2 + \mu)} =: \kappa_q(m). \end{aligned} \tag{5.1}$$

Upon substituting the inequality (5.1) into the equation for H' in (2.1), we derive the inequality

$$H'(t) \geq \kappa_1\kappa_i(m) + \kappa_2\kappa_q(m) - (\gamma_3 + \delta_2 + \mu)H(t),$$

from which we deduce

$$H(t) \geq \frac{\kappa_1\kappa_i(m) + \kappa_2\kappa_q(m)}{\gamma_3 + \delta_2 + \mu} =: \kappa_h(m).$$

Define $\eta(m) := \max\{\frac{S^*+(1-\alpha_1)V_1^*+(1-\alpha_2)V_2^*}{S^*-4m+(1-\alpha_1)(V_1^*-4m)+(1-\alpha_2)(V_2^*-4m)}\}$. For sufficiently large $t \geq t(m)$, from the equations of (2.1), we have

$$\begin{aligned} E'(t) &\geq \beta(t)(\tau_e E(t) + I(t) + \tau(\varepsilon_1 Q(t) + \varepsilon_2 H(t)))\frac{1}{\eta(m)} - (\nu_1 + \nu_2 + \mu)E(t), \\ I'(t) &\geq \nu_1 E(t) - \gamma_1 I(t) - \kappa_1 I(t) - (\delta_1 + \mu)I(t), \\ Q'(t) &\geq \nu_2 E(t) - \kappa_2 Q(t) - \gamma_2 Q(t) - \mu Q(t), \\ H'(t) &\geq \kappa_1 I(t) + \kappa_2 Q(t) - \gamma_3 H(t) - (\delta_2 + \mu)H(t). \end{aligned} \tag{5.2}$$

The system (5.2) can be expressed as

$$\tilde{\mathcal{Y}}'(t) \geq (\frac{F(t)}{\eta(m)} - V(t))\tilde{\mathcal{Y}}(t), \quad \forall t \geqslant t(m), \tag{5.3}$$

with $\tilde{\mathcal{Y}}(t) = \left(\tilde{E}(t), \tilde{I}(t), \tilde{Q}(t), \tilde{H}(t)\right)$. Therefore, the assumptions of ([12], Theorem 4) are satisfied, establishing the persistence of the system (2.1) with respect to E, I, Q, and H. □

6. Existence of positive periodic solutions

Define

$$\mathcal{U} := \Psi,$$
$$\mathcal{U}_0 := \{(S, V_1, V_2, E, I, Q, H, R) \in \mathcal{U} : \ E > 0, \ I > 0, \ Q > 0, \ H > 0\},$$

and

$$\partial\mathcal{U}_0 := \mathcal{U} \setminus \mathcal{U}_0 = \{(S, V_1, V_2, E, I, Q, H, R) \in \mathcal{U} : \ E = 0 \text{ or } I = 0 \text{ or } Q = 0 \text{ or } H = 0\}.$$

Consider the Poincaré map $\mathcal{Q}\colon \mathbb{R}^8_+ \to \mathbb{R}^8_+$ associated with (2.1). Then, for $q^0 \in \mathbb{R}^8_+$, the map is given by $\mathcal{Q}(q^0) = u(\omega, q^0)$, where $u(t, q^0)$ represents the unique solution of (2.1) with the initial condition $q^0 \in \mathcal{U}$.

Lemma 7. *For $\mathcal{R}_0 > 1$, there exists $\chi > 0$ such that, for any $X(0) \in \mathcal{U}_0$ defined in* (2.2) *with $\|X(0) - \mathcal{D}_0\| \leqslant \chi$, the following holds:*

$$\limsup_{m\to\infty} \mathrm{d}\left(\mathcal{Q}^m(X(0)), \mathcal{D}_0\right) \geqslant \chi.$$

Proof. Given $\mathcal{R}_0 > 1$, as indicated by Theorem 3, we ascertain $\rho(\Psi_{F-V}(\omega)) > 1$. Thus, it is possible to choose a sufficiently small $\zeta > 0$ to ensure $\rho(\Psi_{F-V-\mathcal{P}_\zeta}(\omega)) > 1$. The matrix function $\mathcal{P}_\zeta(t)$, sized 4×4, is defined by

$$\mathcal{P}_\zeta(t) = \begin{bmatrix} \tau_e c(t) & c(t) & \tau\epsilon_1 c(t) & \tau\epsilon_2 c(t) \\ 0 & 0 & 0 & 0 \\ 0 & 0 & 0 & 0 \\ 0 & 0 & 0 & 0 \end{bmatrix},$$

where $c(t) = \beta(t)(\zeta + (1 - \alpha_1)\zeta + (1 - \alpha_2)\zeta)$.

In what follows, we claim

$$\limsup_{m\to\infty} \mathrm{d}\left(\mathcal{Q}^m(X(0)), \mathcal{D}_0\right) \geqslant \chi. \tag{6.1}$$

Assume, for the sake of contradiction, that equation (6.1) is false. Then, there exists $X(0) \in \mathcal{U}_0$ such that

$$\limsup_{m\to\infty} \mathrm{d}\left(\mathcal{Q}^m(X(0)), \mathcal{D}_0\right) < \chi. \tag{6.2}$$

For simplicity, let us suppose that

$$\mathrm{d}\left(\mathcal{Q}^m(X(0)), \mathcal{D}_0\right) < \chi, \qquad \forall m \geq 0.$$

Owing to the continuous dependency of the solutions on the initial values, we obtain

$$\|u(s, \mathcal{Q}^m(X(0)) - u(s, \mathcal{D}_0)\| < \zeta, \qquad \forall m \geq 0, \ s \in [0, \omega].$$

Let $t \geqslant 0$ be expressed as $t = m\omega + s$, where $s \in [0, \omega)$ and $m = \left[\frac{t}{\omega}\right]$, representing the largest integer less than or equal to $\frac{t}{\omega}$. Consequently, we can derive

$$\|u(t, X(0)) - u(t, \mathcal{D}_0)\| = \|u(s, \mathcal{Q}^m(X(0))) - u(s, \mathcal{D}_0)\| < \zeta,$$

for all $t \geqslant 0$. This inequality implies $S^* - \zeta \leq S(t) \leq S^* + \zeta$, $V_1^* - \zeta \leq V_1(t) \leq V_1^* + \zeta$, $V_2^* - \zeta \leq V_2(t) \leq V_2^* + \zeta$, $0 \leq E(t) \leq \zeta$, $0 \leq I(t) \leq \zeta$, $0 \leq Q(t) \leq \zeta$, and $0 \leq H(t) \leq \zeta$. Given that $\|X(0) - \mathcal{D}_0\| \leqslant \chi$, we can derive the following:

$$\begin{aligned}
E'(t) &\geq \beta(t)(\tau_e E(t) + I(t) + \tau(\varepsilon_1 Q(t) + \varepsilon_2 H(t)))b(\zeta) - (\nu_1 + \nu_2 + \mu)E(t),\\
I'(t) &\geq \nu_1 E(t) - \gamma_1 I(t) - \kappa_1 I(t) - (\delta_1 + \mu)I(t),\\
Q'(t) &\geq \nu_2 E(t) - \kappa_2 Q(t) - \gamma_2 Q(t) - \mu Q(t),\\
H'(t) &\geq \kappa_1 I(t) + \kappa_2 Q(t) - \gamma_3 H(t) - (\delta_2 + \mu)H(t),
\end{aligned}$$

where $b(\zeta) = \frac{S^* - \zeta + (1-\alpha_1)(V_1^* - \zeta) + (1-\alpha_2)(V_2^* - \zeta)}{N^*}$. To aid our analysis, we consider the following linear system

$$\begin{aligned}
E'(t) &= \beta(t)(\tau_e E(t) + I(t) + \tau(\varepsilon_1 Q(t) + \varepsilon_2 H(t)))b(\zeta) - (\nu_1 + \nu_2 + \mu)E(t),\\
I'(t) &= \nu_1 E(t) - \gamma_1 I(t) - \kappa_1 I(t) - (\delta_1 + \mu)I(t),\\
Q'(t) &= \nu_2 E(t) - \kappa_2 Q(t) - \gamma_2 Q(t) - \mu Q(t),\\
H'(t) &= \kappa_1 I(t) + \kappa_2 Q(t) - \gamma_3 H(t) - (\delta_2 + \mu)H(t).
\end{aligned} \tag{6.3}$$

According to [35, Lemma 2.1], we can establish the existence of a positive, ω-periodic function $p(t)$, making $(E(t), I(t), Q(t), H(t)) = e^{\xi t}p(t)$ a solution to (6.3), where $\xi = \frac{1}{\omega}\ln\rho(\Psi_{F-V+\mathcal{P}_\zeta}(\omega)) > 0$. Given that $\mathcal{R}_0 > 1$ and $\rho(\Psi_{F-V-\mathcal{P}_\zeta}(\omega)) > 1$, it follows that if $(E(0), I(t), Q(0), H(0)) > (0, 0, 0, 0)$, then $(E(t), I(t), Q(t), H(t)) \to \infty$ as $t \to \infty$. Applying the comparison principle [28, Theorem B.1], we deduce $E(0) > 0$, $I(0) > 0$, $Q(0) > 0$, $H(0) > 0$, $\lim_{t\to\infty} E(t) = \infty$, $\lim_{t\to\infty} I(t) = \infty$, $\lim_{t\to\infty} Q(t) = \infty$, and $\lim_{t\to\infty} H(t) = \infty$. However, this contradicts conditions $E(t) < \zeta$, $I(t) < \zeta$, $Q(t) < \zeta$, $H(t) < \zeta$, and Eq (6.2). Consequently, Eq (6.1) holds true, and this concludes the proof. □

Theorem 8. *For $\mathcal{R}_0 > 1$, there exists at least one positive periodic solution to system* (2.1).

Proof. To establish the uniform persistence of $\mathcal{Q}$ with respect to $(\mathcal{U}_0, \partial\mathcal{U}_0)$, we can apply [36, Theorem 3.1.1]. This, in turn, implies the uniform persistence of the solution to (2.1) with respect to $(\mathcal{U}_0, \partial\mathcal{U}_0)$. To begin, let us establish that $\mathcal{U}_0$ and $\partial\mathcal{U}_0$ are positively invariant with respect to the system (2.1). For $X(0) \in \mathcal{U}_0$, solving (2.1) for all $t > 0$, we obtain

$$S(t) = e^{\int_0^t -(\lambda(s)+\theta+\mu)\,ds}\left[S(0) + \Lambda\int_0^t e^{\int_0^s(\lambda(r)+\theta+\mu)\,dr}\,ds\right] > 0, \tag{6.4}$$

$$V_1(t) = e^{\int_0^t -((1-\alpha_1)\lambda(s)+\sigma_1+\mu)\,ds}\left[V_1(0) + \theta\int_0^t S(r)e^{\int_0^r((1-\alpha_1)\lambda(s)+\sigma_1+\mu)\,ds}\,dr\right] > 0, \tag{6.5}$$

$$V_2(t) = e^{\int_0^t -((1-\alpha_2)\lambda(s)+\sigma_2+\mu)\,ds}\left[V_2(0) + \sigma_1\int_0^t V_1(r)e^{\int_0^r((1-\alpha_2)\lambda(s)+\sigma_2+\mu)\,ds}\,dr\right] > 0, \tag{6.6}$$

$$E(t) = e^{-(\nu_1+\nu_2+\mu)t}\left[E(0) + \int_0^t a(s)\lambda(s)e^{(\nu_1+\nu_2+\mu)s}\,ds\right] > 0, \tag{6.7}$$

$$I(t) = e^{-(\gamma_1+\kappa_1+\delta_1+\mu)t}\left[I(0) + \nu_1\int_0^t E(s)e^{(\gamma_1+\kappa_1+\delta_1+\mu)s}\,ds\right] > 0, \tag{6.8}$$

$$Q(t) = e^{-(\gamma_2+\kappa_2+\mu)t}\left[Q(0) + \nu_2\int_0^t E(s)e^{(\gamma_2+\kappa_2+\mu)s}\,ds\right] > 0, \tag{6.9}$$

$$H(t) = e^{-(\gamma_3+\delta_2+\mu)t}\left[H(0) + \int_0^t (\kappa_1 I(s) + \kappa_2 Q(s))e^{(\gamma_3+\delta_2+\mu)s}\,ds\right] > 0, \tag{6.10}$$

$$R(t) = e^{-\mu t}\left[R(0) + \int_0^t (\gamma_1 I(s) + \gamma_2 Q(s) + \gamma_3 H(s) + \sigma_2 V_2(s))e^{\mu s}\,ds\right] > 0, \tag{6.11}$$

where $a(t) = S(t) + (1-\alpha_1)V_1(t) + (1-\alpha_2)V_2(t)$. Therefore, $\mathcal{U}_0$ is confirmed as a positively invariant set. Furthermore, considering the positive invariance of $\mathcal{U}$ and the fact that $\partial\mathcal{U}_0$ is relatively closed within $\mathcal{U}$, we conclude that $\partial\mathcal{U}_0$ is also positively invariant. Furthermore, according to Lemma 1, it is established that the system (2.1) is point dissipative.

Let M_∂ be defined as the set of $\{X(0) \in \partial\mathcal{U}_0 : Q^m(X(0)) \in \partial\mathcal{U}_0,\ \forall m \geqslant 0\}$. We aim to establish that

$$M_\partial = \{(S(0), V_1(0), V_2(0), E(0), I(0), Q(0), H(0), R(0)) : S > 0, V_1 > 0, V_2 > 0, R > 0\}.$$

It is evident that M_∂ includes the set $\{(S(0), V_1(0), V_2(0), E(0), I(0), Q(0), H(0), R(0)) : S > 0, V_1 > 0, V_2 > 0, R > 0\}$. To complete the proof, we need to show that $M_\partial \subset \{(S, V_1, V_2, 0, 0, 0, 0, R) : S > 0, V_1 > 0, V_2 > 0, R > 0\}$, for any initial condition $X(0) \in \partial\mathcal{U}_0$, $E(n\omega) = 0$ or $I(n\omega) = 0$ or $Q(n\omega) = 0$ or $H(n\omega) = 0$, for all $n \geqslant 0$.

Suppose, for the sake of contradiction, that there exists an integer $n_1 \geqslant 0$ such that $E(n_1\omega) > 0$ and $I(n_1\omega) > 0$. Substituting $t = n_1\omega$ for the initial time $t = 0$ into (6.4)–(6.11), we obtain $S(t) > 0$, $V_1(t) > 0$, $V_2(t) > 0$, $E(t) > 0$, $I(t) > 0$, $Q(t) > 0$, $H(t) > 0$, and $R(t) > 0$. However, this contradicts the positive invariance of $\partial\mathcal{U}_0$.

Establishing weak uniform persistence with respect to $(\mathcal{U}_0, \partial\mathcal{U}_0)$ is ensured by Lemma 7. The presence of a global attractor for $\mathcal{Q}$ is guaranteed by Lemma 1. This implies that $\mathcal{D}_0$ serves as an isolated invariant set within $\mathcal{U}$ and $W^s(\mathcal{D}_0) \cap \mathcal{U}_0 = \emptyset$. All solutions within M_∂ converge to $\mathcal{D}_0$, and it is evident that $\mathcal{D}_0$ is acyclic in M_∂. Applying [36, Theorem 1.3.1 and Remark 1.3.1], we can therefore conclude that $\mathcal{Q}$ exhibits uniform (strong) persistence with respect to $(\mathcal{U}_0, \partial\mathcal{U}_0)$. Consequently, there exists an $\varepsilon > 0$ such that

$$\liminf_{t\to\infty} (E(t), I(t), Q(t), H(t))^T \geqslant (\varepsilon, \varepsilon, \varepsilon, \varepsilon)^T$$

for all $X(0) \in \mathcal{U}_0$. Invoking [36, Theorem 1.3.6], we determine the existence of a fixed point $\bar{X}(0) \in \mathcal{U}_0$ for $\mathcal{Q}$. Consequently, system (2.1) has at least one periodic solution $u(t, \bar{X}(0))$, where $\bar{X}(0) = (\bar{S}(0), \bar{V}_1(0), \bar{V}_2(0), \bar{E}(0), \bar{I}(0), \bar{Q}(0), \bar{H}(0), \bar{R}(0)) \in \mathcal{U}_0$. To establish that $\bar{S}(0)$ is positive, consider the scenario where $\bar{S}(0) = 0$. In this case, it is inferred that $\bar{S}(0) > 0$ for all $t > 0$. However, by exploiting the periodicity of the solution, a contradiction arises with $\bar{S}(0) = \bar{S}(n\omega) = 0$. □

7. Model calibration and sensitivity analysis

In order to verify and strengthen our analytical results, we apply our seasonal compartmental mathematical model to real measles data from two Asian countries. Measles, an infectious disease, presents substantial public health and economic challenges throughout the world. Despite the limitations of testing, quarantine, and isolation measures it has been effective in controlling the spread

of diseases [37, 38]. These measures play a crucial role in reducing the risk of infection and preventing the future prevalence of the disease. Vaccination is essential for the management of infectious diseases, but many vaccines are imperfect, with partial protective effects and trade-offs between transmission and recovery [37, 38]. The efficacy of a vaccine and the population turnover rate play crucial roles in disease eradication. The results of vaccination games depend on factors such as the dynamics of disease transmission, the cost of infection, and the efficacy of the vaccine. It is important to consider the imperfections of vaccines in disease models, especially for diseases with high basic reproduction numbers.

Within this section, our focus turns to investigating the spread of measles as a case study in two different countries: Saudi Arabia from August 2018 to August 2021 and Pakistan from January 2019 to December 2021, as documented by the World Health Organization (WHO) [39], using our established model. The simulation results presented aim to illustrate the performance of our model with periodic parameters in capturing seasonal fluctuation data. With reference to [7, 17, 40–42], we assume that the transmission rate $\beta(t)$ follows a time-periodic pattern with a period of 12 months. This is mathematically expressed as $\beta(t) = \beta_0 \cdot \left(a + b \sin\left(c + \frac{2\pi t}{12}\right)\right)$. Here, a and b function as adjustable parameters, c denotes the amplitude of the forcing, and β_0 signifies the baseline value of the time-dependent contact rate.

7.1. Parameters estimation and curve fitting to measles data from Saudi Arabia and Pakistan

The World Bank report on Saudi Arabia [43] in 2021 indicates a total population of 36, 408, 820 with a life expectancy at birth of 77 years. This results in a monthly birth rate of approximately $\Lambda = \mu \times N = 39,403$, where μ is determined as $1/(12 \times 77)$. Similarly, World Bank data for Pakistan [44] reveals a total population of 231, 402, 117 in 2021, with a life expectancy at birth of 66 years. Applying the same calculation, the estimated monthly human birth population in Pakistan is approximately 292, 174, with μ calculated as $1/(12 \times 66)$. A single administration of the MMR (Measles, Mumps, and Rubella) vaccine demonstrates an efficacy of around 93% in preventing measles, while two doses of the vaccine exhibits an efficacy of approximately 97%, as reported by both the WHO [45] and the Centers for Disease Control and Prevention (CDC) [46]. Consequently, the assumed values for the efficacy of the vaccine are denoted as $\alpha_1 = 0.93$ for a single dose and $\alpha_1 = 0.97$ for two doses. Applying Latin hypercube sampling alongside the least squares method, we aim to estimate the parameters of the model (2.1) to obtain the optimal fit with the given data. This sampling technique allows for the simultaneous evaluation of variance in multiple parameter values, as outlined in [34].

Fitting our model (2.1) to confirmed measles cases in Saudi Arabia from August 2018 to August 2021 and in Pakistan from January 2019 to December 2021 allowed us to obtain estimates for the parameters of the measles model. Although certain parameter values were drawn from existing literature to inform our initial estimates, the remaining parameters were determined through the process of fitting the model to the observed data.

Figure 2 presents the fit of the model with data on measles (cumulative cases and new cases) from Saudi Arabia between 2018 and 2021, showing a reasonably good fit and a high goodness of fit $R^2 = 0.95961$. Using the method established in [32], we numerically estimated the current basic reproduction number as $\mathcal{R}_0 \approx 0.585887 < 1$, signifying the extinction of the disease in Saudi Arabia.

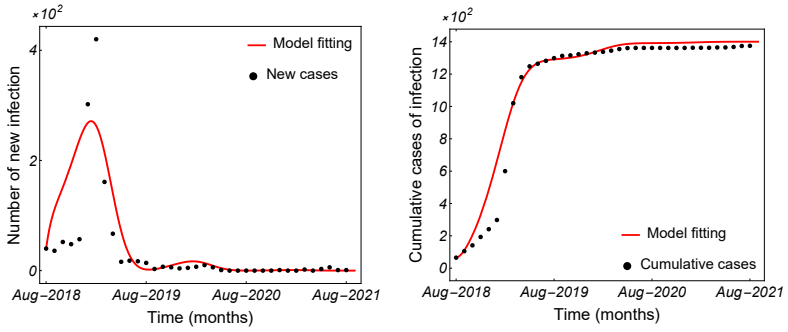

Figure 2. Best-fitting results of model (2.1) to the data from Saudi Arabia for newly infected cases (**left**) and cumulative infected cases (**right**) between 2018 and 2021, using parameters from Table 2 (Saudi Arabia).

Table 2. Parameters for model (2.1) providing the best fit.

Parameters	Values Pakistan	Values Saudi Arabia	Units	Sources
Λ	292174	39403	Persons Month^{-1}	[44,47]
μ	0.00126263	0.00108225	Month^{-1}	[44,47]
β_0	0.476	0.484	Person^{-1} Month^{-1}	Fitted
a	1.14	2.36	–	Fitted
b	1.99	6.78	–	Fitted
c	8.88	4.82	–	Fitted
τ_e	0	0	Month^{-1}	Assumed
τ	0.841	0.469	Month^{-1}	Fitted
α_1	0.93	0.93	–	[45,46]
α_2	0.97	0.97	–	[45,46]
ϵ_1	0.743	0.816	–	Fitted
ϵ_2	0.699	0.611	–	Fitted
σ_1, σ_2	0.047, 0.028	0.047, 0.028	Month^{-1}	[48]
θ	0.000154	0.000154	Month^{-1}	Fitted
ν_1	0.308	0.268	Month^{-1}	[37,38]
ν_2	0.352	0.264	Month^{-1}	[37,38]
κ_1	0.2	0.226	Month^{-1}	Fitted
κ_2	0.252	0.22	Month^{-1}	Fitted
γ_1	0.1	0.29	Month^{-1}	[37,38]
γ_2	0.3	0.518	Month^{-1}	[37,38]
γ_3	0.1	0.344	Month^{-1}	[37,38]
δ_1, δ_2	0.0365, 0.0465	0.0365, 0.0465	Month^{-1}	[49]
$\mathcal{R}_0$	4.05938	0.585887	–	Estimated

On the contrary, Figure 3 shows the fit of the model with Pakistan's measles data between 2019 and 2021, also showing a reasonably good fit and a high goodness of fit $R^2 = 0.972413$, indicating its ability to capture key patterns of incidence of measles epidemics during 2019-2021. Once again, we estimate $\mathcal{R}_0 \approx 4.05938 > 1$, which reveals the persistence of the disease in Pakistan. This demonstrates that our model (2.1) is capable of reproducing the two types of outcomes observed in the measles

epidemic in Asia.

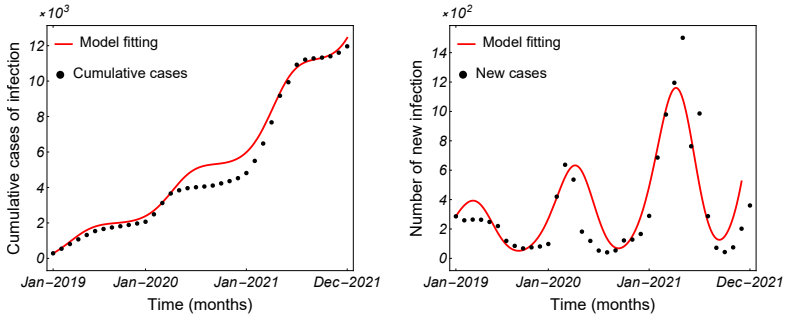

Figure 3. Best-fitting results of model (2.1) to the data from Pakistan for cumulative infected cases (**left**) and newly infected cases (**right**) between 2019 and 2021, using parameters from Table 2 (Pakistan).

7.2. Sensitivity analysis of the time–average reproduction number

Performing a sensitivity analysis on the basic reproductive number $\mathcal{R}_0$, our aim is to quantify the variations in the parameters of the model given in Eq (2.1). This analysis helps identify parameters that significantly influence both the basic reproduction number and disease transmission dynamics. Given that our main focus lies in determining the basic reproduction number ($\mathcal{R}_0$) of the periodic model (2.1), which lacks an explicit expression for $\mathcal{R}_0$ defined as the spectral radius of a linear operator, we will employ the following remark to derive a formula for the time–average reproduction number ($\langle\mathcal{R}_0\rangle$) of the associated nonautonomous system (see [32] for more details).

Remark 9. *In accordance with the notation provided in [32], the integral average of a continuous function $f(t)$, which exhibits periodicity with a period of ω, can be defined as $\langle f\rangle := \frac{1}{\omega}\int_0^\omega f(t)\,dt$.*

By applying the findings derived from the study conducted by [50], we obtain

$$\langle F\rangle = \begin{bmatrix} \tau_e\langle\beta\rangle L^* & \langle\beta\rangle L^* & \tau\epsilon_1\langle\beta\rangle L^* & \tau\epsilon_2\langle\beta\rangle L^* \\ 0 & 0 & 0 & 0 \\ 0 & 0 & 0 & 0 \\ 0 & 0 & 0 & 0 \end{bmatrix},$$

and

$$V = \begin{bmatrix} \nu_1+\nu_2+\mu & 0 & 0 & 0 \\ -\nu_1 & \gamma_1+\kappa_1+\delta_1+\mu & 0 & 0 \\ -\nu_2 & 0 & \gamma_2+\kappa_2+\mu & 0 \\ 0 & -\kappa_1 & -\kappa_2 & \gamma_3+\delta_2+\mu \end{bmatrix},$$

where $L^* = \frac{S^*+(1-\alpha_1)V_1^*+(1-\alpha_2)V_2^*}{N^*}$. Hence, we get

$$\langle\mathcal{R}_0\rangle = \rho(\langle F\rangle V^{-1}) = \langle\mathcal{R}_E\rangle + \langle\mathcal{R}_I\rangle + \langle\mathcal{R}_Q\rangle + \langle\mathcal{R}_H\rangle, \tag{7.1}$$

where

$$\langle\mathcal{R}_E\rangle = \frac{\langle\beta\rangle\tau_e L^*}{\mu+\nu_1+\nu_2}, \quad \langle\mathcal{R}_I\rangle = \frac{\langle\beta\rangle\nu_1 L^*}{(\gamma_1+\delta_1+\kappa_1+\mu)(\mu+\nu_1+\nu_2)}, \quad \langle\mathcal{R}_Q\rangle = \frac{\langle\beta\rangle\epsilon_1\nu_2\tau L^*}{(\gamma_2+\kappa_2+\mu)(\mu+\nu_1+\nu_2)},$$

$$\langle \mathcal{R}_H \rangle = \frac{\langle \beta \rangle \epsilon_2 \tau L^*}{(\gamma_3 + \delta_2 + \mu)(\mu + \nu_1 + \nu_2)} \left(\frac{\kappa_1 \nu_1}{\gamma_1 + \delta_1 + \kappa_1 + \mu} + \frac{\kappa_2 \nu_2}{\gamma_2 + \kappa_2 + \mu} \right).$$

The use of sensitivity indices is a common practice in sensitivity analysis, as elucidated in [51]. The normalized forward sensitivity index for a variable concerning a parameter is determined by calculating the ratio between the relative change in the variable and the relative change in the parameter. Specifically, the normalized forward sensitivity index of $\langle \mathcal{R}_0 \rangle$ with respect to a parameter x is defined as

$$\Upsilon_x^{\langle \mathcal{R}_0 \rangle} = \frac{x}{\langle \mathcal{R}_0 \rangle} \times \frac{\partial \langle \mathcal{R}_0 \rangle}{\partial x}.$$

We conducted a sensitivity analysis for the time-averaged reproduction number $\langle \mathcal{R}_0 \rangle$, as defined in Eq (7.1). Our investigation, as depicted in Figure 4, reveals that $\langle \mathcal{R}_0 \rangle$ exhibits heightened sensitivity to variations in the infection rate ($\langle \beta \rangle$), relative transmissibility (τ and τ_e), and recovery rates (γ_1 and γ_3). Turning our attention to Figure 5, we present the sensitivity indices for $\langle \mathcal{R}_E \rangle$, $\langle \mathcal{R}_I \rangle$, $\langle \mathcal{R}_Q \rangle$, and $\langle \mathcal{R}_H \rangle$. This visualization allows for a comprehensive understanding of the factors that influence these specific reproduction numbers, providing a nuanced perspective on their sensitivities to parameters such as infection rate, relative transmissibility, and recovery rates.

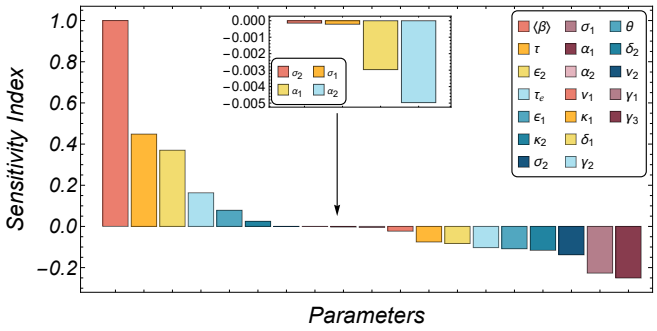

Figure 4. Sensitivity analysis for $\langle \mathcal{R}_0 \rangle$.

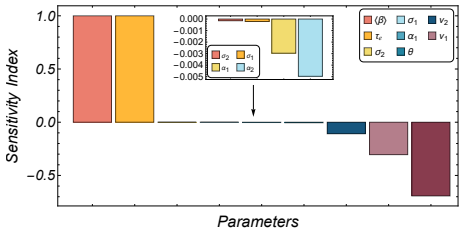

(a) Sensitivity Analysis for $\langle \mathcal{R}_E \rangle$.

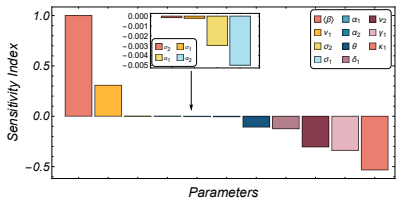

(b) Sensitivity Analysis for $\langle \mathcal{R}_I \rangle$.

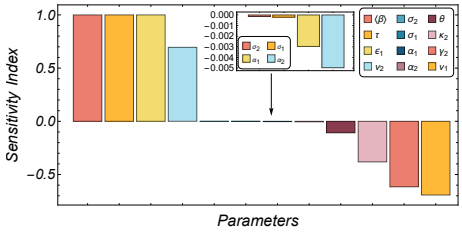

(c) Sensitivity Analysis for $\langle \mathcal{R}_Q \rangle$.

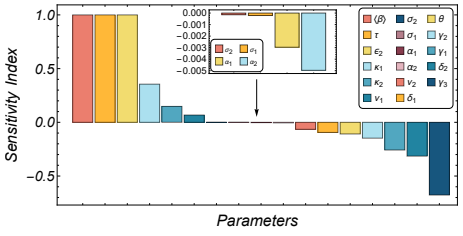

(d) Sensitivity Analysis for $\langle \mathcal{R}_H \rangle$.

Figure 5. Sensitivity analysis for $\langle \mathcal{R}_E \rangle$, $\langle \mathcal{R}_I \rangle$, $\langle \mathcal{R}_Q \rangle$, and $\langle \mathcal{R}_H \rangle$.

By setting the time-varying transmission rate to a constant value, $\beta(t) = \beta_0$, one can derive a formula for the basic reproduction number of the autonomous version of system (2.1). Referring to (7.1), we obtain

$$\mathcal{R}_0^a = \frac{\beta_0 \tau_e L^*}{\mu + \nu_1 + \nu_2} + \frac{\beta_0 \nu_1 L^*}{(\gamma_1 + \delta_1 + \kappa_1 + \mu)(\mu + \nu_1 + \nu_2)} + \frac{\beta_0 \epsilon_1 \nu_2 \tau L^*}{(\gamma_2 + \kappa_2 + \mu)(\mu + \nu_1 + \nu_2)},$$
$$\frac{\beta_0 \epsilon_2 \tau L^*}{(\gamma_3 + \delta_2 + \mu)(\mu + \nu_1 + \nu_2)} \left(\frac{\kappa_1 \nu_1}{\gamma_1 + \delta_1 + \kappa_1 + \mu} + \frac{\kappa_2 \nu_2}{\gamma_2 + \kappa_2 + \mu} \right).$$

Figure 6 depicts the curves of the basic reproduction number $\mathcal{R}_0^a$ of the autonomous version of system (2.1), the time-averaged reproduction number $\langle \mathcal{R}_0 \rangle$ and the the basic reproduction number $\mathcal{R}_0$ plotted in relation to certain parameters of the system (2.1). Specifically, these parameters include the average transmission rate ($\langle \beta \rangle$), relative transmissibility (τ and τ_e), quarantine rate for exposed individuals (ν_2), recovery rate for infectious individuals (γ_1), and vaccine coverage rate (θ). This visual representation of the curve in relation to these system parameters improves our understanding of how they collectively influence the potential for disease transmission.

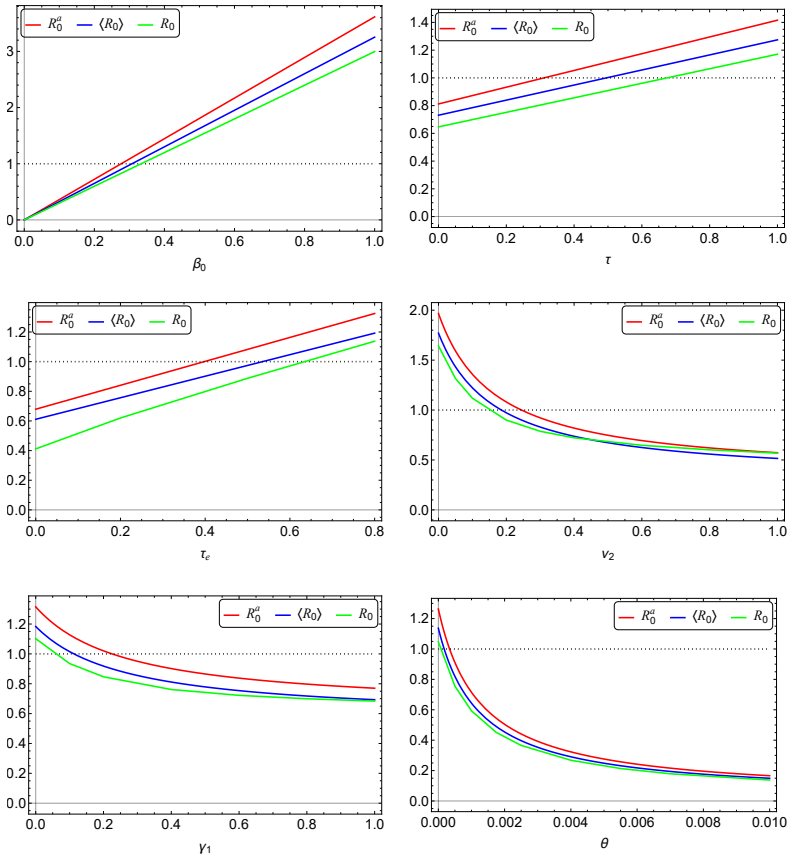

Figure 6. The curves of the basic reproduction number $\mathcal{R}_0^a$ of the autonomous model, the time-averaged reproduction number $\langle \mathcal{R}_0 \rangle$, and the basic reproduction number $\mathcal{R}_0$ are plotted with respect to some of the system (2.1) parameters, namely, β_0, τ, τ_e, ν_2, γ_1, and θ.

The calculations show that $\mathcal{R}_0^a > \langle \mathcal{R}_0 \rangle \geq \mathcal{R}_0$, suggesting that $\mathcal{R}_0^a$ and $\langle \mathcal{R}_0 \rangle$ overestimate the risk of disease transmission. It is worth noting that several papers have addressed the issue of underestimation

and overestimation of the average basic reproduction number. For instance, it was demonstrated in [11, 17,25] that $\mathcal{R}_0 > [\mathcal{R}_0]$, whereas in [26], the authors provided an example where $\mathcal{R}_0 < [\mathcal{R}_0]$. More details can also be found in [11, 52].

8. Numerical simulations

This section is dedicated to presenting numerical simulations. The aim is to both illustrate and validate the theoretical findings discussed earlier. Through these simulations, we provide visual evidence that demonstrates the alignment between our time-periodic model and the observed seasonal fluctuations.

8.1. Extinction and persistence

It is clear from the exposition in Section 4 until Section 6 that the parameter $\mathcal{R}_0$ plays a significant role in determining whether the disease will persist in the population, as elucidated by Theorems 5 and 8. Theorem 8 asserts that if $\mathcal{R}_0 > 1$, the dynamical system (2.1) possesses a positive ω-periodic solution. To show the persistence of the disease and the existence of the periodic solution, we set the parameter values as follows: $a = 0.9$, $\beta_0 = 0.312$, $b = 8.6$, $c = 1.7$, $\alpha_1 = 0.93$, $\alpha_2 = 0.5$, $\gamma_1 = 0.1$, $\gamma_2 = 0.3$, $\gamma_3 = 0.1$, $\delta_1 = 0.0365$, $\delta_2 = 0.0465$, $\epsilon_1 = 0.523$, $\epsilon_2 = 0.474$, $\theta = 0.000154$, $\kappa_1 = 0.231$, $\kappa_2 = 0.203$, $\nu_1 = 0.166$, $\nu_2 = 0.178$, $\sigma_1 = 0.047$, $\sigma_2 = 0.028$, $\tau_e = 0.556$, and $\tau = 0.523$. To further elaborate on the profound implications of this result, Figures 7–9 offer vivid illustrations of the long-term behavior and the enduring presence of measles, along with the existence of periodic positive solutions when $\mathcal{R}_0 \approx 1.12776 > 1$. Consequently, disease compartments not only persist, but also evolve into an endemic state within the population, characterized by recurring annual outbreaks.

Figures 10 and 11 provide visual representations that effectively corroborate the theoretical findings. These findings show that the disease-free equilibrium $\mathcal{D}_0$ demonstrates global asymptotic stability when $\mathcal{R}_0 = 0.474236 < 1$. As a result, it can be inferred that the disease can be eliminated if $\mathcal{R}_0 < 1$.

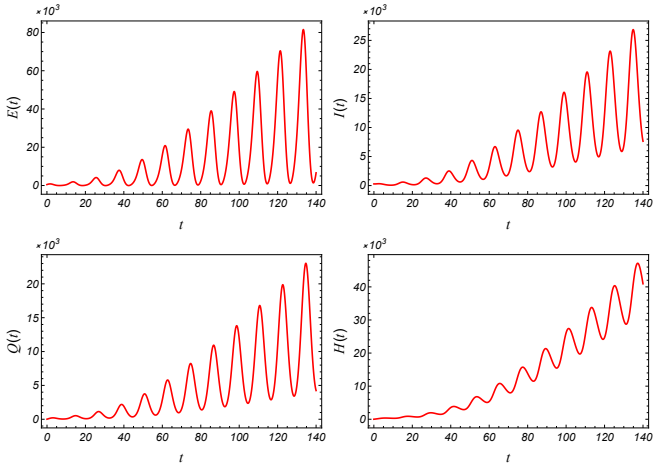

Figure 7. Persistence of measles when $\mathcal{R}_0 = 1.12776 > 1$.

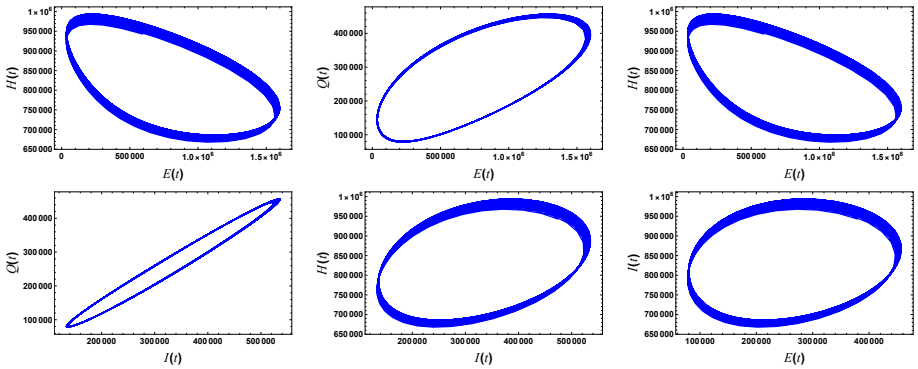

Figure 8. The existence of positive periodic solutions when $\mathcal{R}_0 = 1.12776 > 1$.

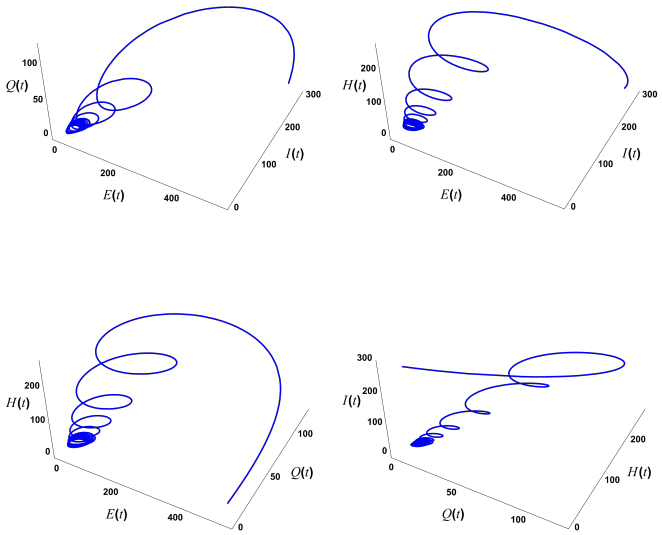

Figure 9. The existence of positive periodic solutions when $\mathcal{R}_0 = 1.12776 > 1$.

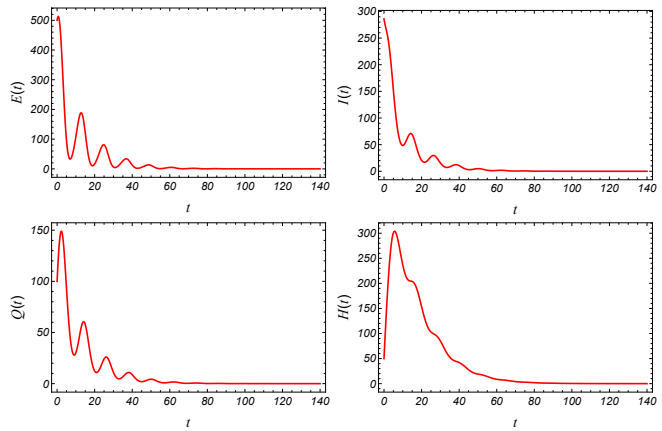

Figure 10. Extinction of measles when $\beta_0 = 0.131$ and $\mathcal{R}_0 = 0.474236 < 1$.

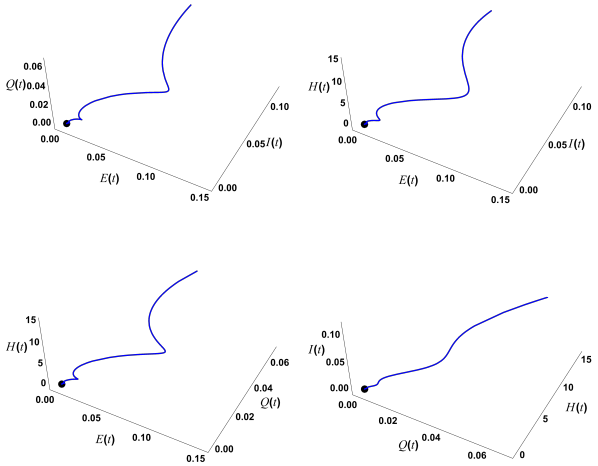

Figure 11. Global asymptotic stability of $\mathcal{D}_0$ when $\beta_0 = 0.131$ and $\mathcal{R}_0 = 0.474236 < 1$.

8.2. Examining the impact of imperfect quarantine and isolation

Imperfect quarantine and isolation can significantly impact the spread of measles. It is crucial to acknowledge that the effects of quarantine and isolation can vary based on the specific characteristics of the disease and the population studied. In this study, we investigate the influence of imperfect quarantine and isolation on the spread of measles in Pakistan, using parameter values fitted to the measles data presented in Table 2.

To predict and estimate the impact of quarantine and isolation on future measles outbreaks in Pakistan, simulations were started using parameters fitted up to month 35, with subsequent adjustments. Different values of the quarantine efficacy modification parameter, ϵ_1, are illustrated in Figure 12, while the isolation efficacy modification parameter, ϵ_2, is shown in Figure 13. The results indicate that the imperfect implementation of quarantine and isolation, particularly when $\epsilon_2 = 1 = \epsilon_2$, may lead to a substantial increase in the number of measles infectious populations. On the contrary, the perfect implementation of quarantine with $\epsilon_1 = 0$ decreases the number of infectious individuals without causing extinction. Perfect isolation, observed when $\epsilon_2 = 0$, leads to a significant decrease in the number of infectious individuals, leading to extinction. These findings underscore the importance of implementing perfect quarantine and isolation measures.

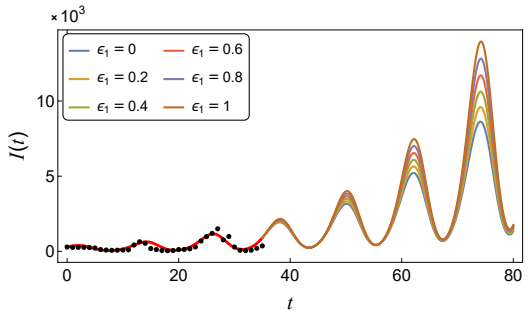

Figure 12. Variations in the infectious population under different values of the quarantine efficacy modification parameter, ϵ_1, using the parameter values listed in Table 2 (Pakistan).

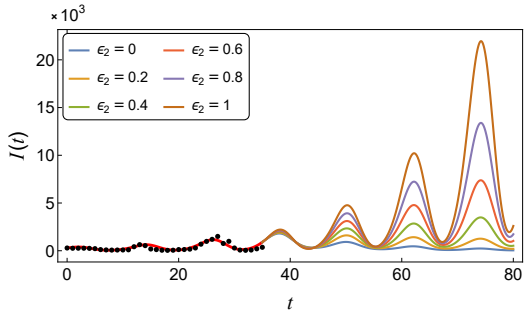

Figure 13. Variations in the infectious population under different values of the isolation efficacy modification parameter, ϵ_2, using the parameter values listed in Table 2 (Pakistan).

8.3. Examining the impact of imperfect vaccination

The impact of incomplete first- and second-dose vaccination on measles is a significant concern for public health. Incomplete coverage, suboptimal vaccine efficacy, and deviations from recommended dose schedules can undermine the effectiveness of vaccination efforts. As seen in Figure 14, when the vaccination coverage rate (θ) improves, the impact of the measles epidemic decreases. This can be a challenge to achieve in countries like Pakistan.

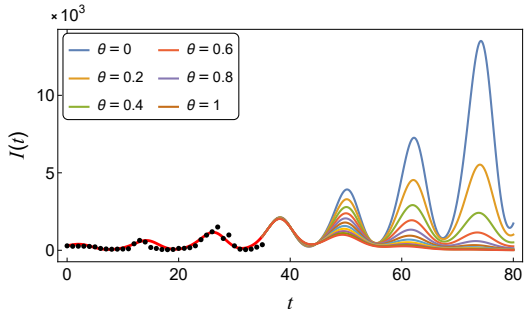

Figure 14. Variations in the infectious population under different values of the vaccine coverage rate, θ, using the parameter values listed in Table 2 (Pakistan).

While the effectiveness of a vaccine is crucial in managing the spread of diseases, its impact can vary depending on the basic reproduction number of the disease. Diseases with lower basic reproduction numbers may show minimal differences in outcomes between perfect and imperfect vaccines. In contrast, diseases with higher basic reproduction numbers, such as measles, pose greater challenges when faced with an imperfect vaccine. The presence of imperfections in vaccine efficacy can cause increased difficulties in achieving effective disease control measures.

To address the challenge of measles control, the government could prioritize improving the efficacy of vaccines (α_1 and α_2), as illustrated in Figures 15 and 16. At the same time, it is crucial to ensure accessibility for individuals in poverty. In particular, achieving a high coverage rate (θ) for the vaccine, coupled with elevated efficacy rates (α_1 and α_2), proves paramount. A higher efficacy rate plays a crucial role in decreasing the number of infectious cases, highlighting its importance in alleviating the impact of the measles epidemic.

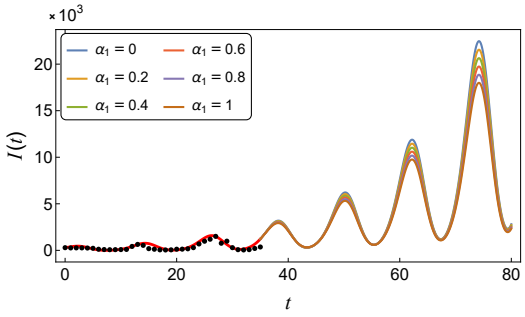

Figure 15. Variations in the infectious population under different values of the first dose vaccine efficacy parameter, α_1, using the parameter values listed in Table 2 (Pakistan).

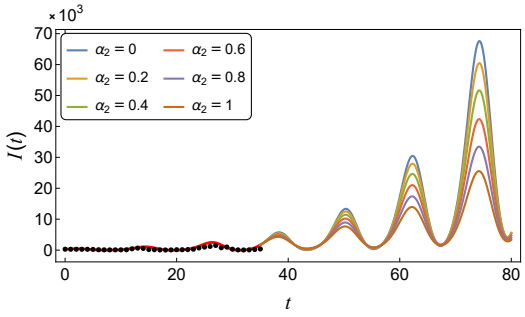

Figure 16. Variations in the infectious population under different values of the second dose vaccine efficacy parameter, α_2, using the parameter values listed in Table 2 (Pakistan).

9. Discussion

This study delves into the intricacies of a nonautonomous mathematical model designed to elucidate the transmission dynamics of infectious diseases over time. By incorporating a seasonal transmission parameter and imperfections in quarantine, isolation, and vaccination strategies, the model builds on previous works such as [17, 19] to explore threshold dynamics that govern disease persistence or elimination. Through a comprehensive analysis of the basic reproduction number ($\mathcal{R}_0$), the research establishes its pivotal role as a threshold parameter, delineating the conditions under which the disease-free equilibrium is globally stable or the disease persists. The complexity of the model lies in its integration of time-dependent coefficients and the interplay of quarantine, isolation, and vaccination measures, allowing a nuanced understanding of the dynamics of the disease. This study differs from [17], which employed a mathematical model with a seasonal transmission parameter and a double-dose vaccination to examine the spread of measles over time, assuming that only the first dose of the vaccine was imperfect. In contrast, our study assumes imperfections in both the first and second doses of the vaccine. Additionally, we incorporate the impact of imperfect interventions, specifically quarantine, isolation, and vaccination.

Using real-world measles data from two Asian countries, our seasonal compartmental mathematical model validates and supports our analytical results. The research focuses on examining measles dynamics in Saudi Arabia and Pakistan, incorporating essential factors such as vaccination, time-varying transmission rates, and imperfections in control strategies. By calibrating the model

with real-world data, the dynamics of the disease are successfully captured. Key parameters such as vaccine efficacy (α_1 and α_2) and time-dependent transmission rates were crucial to accurately reproduce observed patterns and estimate critical parameters. Numerical simulations highlighted the importance of the basic reproduction number ($\mathcal{R}_0$) in determining the persistence of the disease. Measles demonstrated persistence when $\mathcal{R}_0 > 1$ and tended toward extinction when $\mathcal{R}_0 < 1$. Sensitivity analysis emphasized the importance of effective quarantine, isolation, and vaccination strategies in the control of infectious populations. Our sensitivity analysis of the time-averaged reproduction number, $\langle \mathcal{R}_0 \rangle$, in a periodic model revealed a significant sensitivity to key parameters such as infection rate, relative transmissibility, and recovery rates. The formula derived for $\langle \mathcal{R}_0 \rangle$ allowed for a comprehensive understanding of its contributions from exposed, infectious, quarantined, and hospitalized individuals. Visualizations of the sensitivity indices provided information on the influence of specific parameters on different reproduction numbers, helping to prioritize interventions as shown in Figures 4 and 5. The graphical representation of the curves of the basic reproduction number $\mathcal{R}_0^a$ of the autonomous model, the time-averaged reproduction number $\langle \mathcal{R}_0 \rangle$, and the basic reproduction number $\mathcal{R}_0$ in relation to the system parameters further improved our understanding of its impact on the potential for disease transmission as shown in Figure 6. In general, this analysis provides valuable information to inform interventions and guide future research in infectious disease modeling.

The numerical simulations conducted in this study serve to validate and illustrate the theoretical insights discussed earlier on the dynamics of measles in a population. The visual evidence presented in Figures 7, 9, 10, and 11 aligns with the theoretical findings, emphasizing the pivotal role of the basic reproduction number ($\mathcal{R}_0$) in determining the long-term behavior of measles. When $\mathcal{R}_0$ exceeds 1, the simulations demonstrate the persistence of measles in the population, accompanied by the existence of periodic positive solutions. In contrast, when $\mathcal{R}_0$ falls below 1, the disease-free equilibrium is globally asymptotically stable, leading to the extinction of measles. These results provide valuable information on the conditions under which measles can establish and persist within a population or face elimination. Examining imperfect quarantine, isolation, and vaccination further illuminates the practical implications for disease control. Simulations indicate that the effective implementation of quarantine and isolation measures is crucial to curtailing the spread of measles, highlighting the sensitivity of the model to variations in the parameters of efficacy modification. Furthermore, the impact of imperfect vaccination, considering coverage rates and vaccine efficacy, underscores the importance of these factors in mitigating the burden of measles. These results are important for understanding the variations in the infectious population due to the overestimation/underestimation of the disease transmission risk provided by the basic reproduction numbers of the autonomous system as shown in Figure 6.

Looking forward, future research should explore the long-term impact of vaccination campaigns in dynamic epidemiological landscapes. Incorporating real-time data and refining models based on ongoing observations, considering the time delay between the first and second doses, as well as the time to arrive in the recovered state after receiving the second dose of the vaccine, will improve predictive accuracy. Addressing uncertainties in parameter estimates and evaluating the effectiveness of new vaccines are crucial for future research.

Use of AI tools declaration

The author declare they have not used Artificial Intelligence (AI) tools in the creation of this article.

Acknowledgments

M.A.I. was supported by the project No. 146210, implemented with the support provided from the National Research, Development and Innovation Fund of Hungary, financed under the PD_23 funding scheme, by the National Laboratory for Health Security, RRF-2.3.1-21-2022-00006 and by the project No. 129877, implemented with the support provided from the National Research, Development and Innovation Fund of Hungary, financed under the KKP_19 funding scheme. This publication is funded by University of Szeged Open Access Fund (grant number: 6993).

Conflict of interest

The author declares no conflict of interest.

References

1. A. Zobayer, M. S. Ullah, K. Ariful Kabir, A cyclic behavioral modeling aspect to understand the effects of vaccination and treatment on epidemic transmission dynamics, *Sci. Rep.*, **13** (2023), 8356. https://doi.org/10.1038/s41598-023-35188-3
2. M. J. Plank, S. C. Hendy, R. N. Binny, G. Vattiato, A. Lustig, O. J. Maclaren, Using mechanistic model-based inference to understand and project epidemic dynamics with time-varying contact and vaccination rates, *Sci. Rep.*, **12** (2022), 20451. https://doi.org/10.1038/s41598-022-25018-3
3. Y. Wei, J. Guan, Y. Zhao, F. Chen, Progress and perspective of transmission dynamics models in prevention and control of infectious diseases, In: *Ye, DQ. (eds) Progress in China Epidemiology*, Singapore: Springer, 2022. https://doi.org/10.1007/978-981-19-2199-5_22
4. J. Tanimoto, Quarantine and isolation, In: *Sociophysics Approach to Epidemics. Evolutionary Economics and Social Complexity Science*, Singapore: Springer, **23** (2021). https://doi.org/10.1007/978-981-33-6481-3_5
5. M. A. Safi, A. B. Gumel, Mathematical analysis of a disease transmission model with quarantine, isolation and an imperfect vaccine, *Comput. Math. Appl.*, **61** (2011), 3044–3070. https://doi.org/10.1016/j.camwa.2011.03.095
6. M. A. Safi, Mathematical analysis of the role of quarantine and isolation in epidemiology, Ph.D thesis, *Department of Mathematics, University of Manitoba*, 2010.
7. K. Dietz, The incidence of infectious diseases under the influence of seasonal fluctuations, In: *Mathematical Models in Medicine Workshop*, Mainz: Springer, 1976. https://doi.org/10.1016/j.camwa.2011.03.095
8. K. F. Nipa, L. J. Allen, The effect of demographic variability and periodic fluctuations on ddisease outbreaks in a Vector-Host epidemic model, *In: Teboh-Ewungkem, M.I., Ngwa, G.A. (eds) Infectious Diseases and Our Planet. Mathematics of Planet Earth*, Cham: Springer, **7** (2021), 15–35. https://doi.org/10.1007/978-3-030-50826-5_2

9. J. Rashidinia, M. Sajjadian, J. Duarte, C. Januário, N. Martins, On the dynamical complexity of a seasonally forced discrete SIR epidemic model with a constant vaccination strategy, *Complexity,* **2018** (2018), 7191487. https://doi.org/10.1155/2018/7191487
10. H. Sun, H. Li, Z. Zhu, Dynamics of an SIRS epidemic model with periodic infection rate on a scale-free network, *J. Biolog. Sys.*, **30** (2022), 673–693. https://doi.org/10.1142/S0218339022500243
11. W. Wang, X. Q. Zhao, Threshold dynamics for compartmental epidemic models in periodic environments, *J. Dyn. Diff. Equat.*, **20** (2008), 699–717. https://doi.org/10.1007/s10884-008-9111-8
12. C. Rebelo, A. Margheri, N. Bacaër, Persistence in seasonally forced epidemiological models, *J. Math. Biol.*, **64** (2012), 933–949. https://doi.org/10.1007/s00285-011-0440-6
13. T. Zhang, Z. Teng, S. Gao, Threshold conditions for a nonautonomous epidemic model with vaccination, *Appl. Anal.*, **87** (2008), 181–199. https://doi.org/10.1080/00036810701772196
14. C. M. Silva, A nonautonomous epidemic model with general incidence and isolation, *Math. Meth. Appl. Sci.*, **37** (2014), 1974–1991. https://doi.org/10.1002/mma.2950
15. Z. Guo, F. B. Wang, X. Zou, Threshold dynamics of an infective disease model with a fixed latent period and non-local infections, *J. Math. Biol.*. **65** (2012), 1387–1410. https://doi.org/10.1007/s00285-011-0500-y
16. M. A. Ibrahim, A. Dénes, A mathematical model for Lassa fever transmission dynamics in a seasonal environment with a view to the 2017–20 epidemic in Nigeria, *Nonlinear Anal.: Real World Appl.*, **60** (2021), 103310. https://doi.org/10.1016/j.nonrwa.2021.103310
17. M. A. Ibrahim, A. Dénes, Stability and threshold dynamics in a seasonal mathematical model for measles outbreaks with double-dose vaccination, *Mathematics*, **11** (2023), 1791. https://doi.org/10.3390/math11081791
18. L. Lou, X. Q. Zhao, Threshold dynamics in a time-delayed periodic SIS epidemic model, *Discrete Cont. Dyn. Sys. Ser. B*, **126** (2009), 169–186. 10.3934/dcdsb.2009.12.169
19. M. A. Safi, M. Imran, A. B. Gumel, Threshold dynamics of a nonautonomous SEIRS model with quarantine and isolation, *Theory Biosci.*, **131** (2012), 19–30. https://doi.org/10.1007/s12064-011-0148-6
20. D. Aldila, D. Asrianti, A deterministic model of measles with imperfect vaccination and quarantine intervention, *J. Phys.: Conf. Ser.*, **1218** (2019), 012044. https://doi.org/10.1088/1742-6596/1218/1/012044
21. M. Erdem, M. Safan, C. Castillo-Chavez, Mathematical analysis of an SIQR influenza model with imperfect quarantine, *Bull. Math. Biol.*, **79** (2017), 1612–1636. https://doi.org/10.1007/s11538-017-0301-6
22. Z. Feng, Final and peak epidemic sizes for seir models with quarantine and isolation, *Math. Biosci. Eng.*, **4** (2007), 675–686. https://doi.org/10.3934/mbe.2007.4.675
23. Z. Memon, S. Qureshi, B. R. Memon, Mathematical analysis for a new nonlinear measles epidemiological system using real incidence data from Pakistan, *Eur. Phys. J. Plus*, **135** (2020), 675–686. https://doi.org/10.1140/epjp/s13360-020-00392-x

24. S. Opoku, B. Seidu, P. N. Akuka, A mathematical analysis of the impact of maternally derived immunity and double-dose vaccination on the spread and control of measles, *Comput. Math. Biophys.*, **11** (2023), 20230106. https://doi.org/10.1515/cmb-2023-0106
25. M. A. Ibrahim, A. Dénes, Threshold dynamics in a model for Zika virus disease with seasonality, *Bull. Math. Biol.*, **83** (2021), 27. https://doi.org/10.1007/s11538-020-00844-6
26. L. Liu, X. Q. Zhao, Y. Zhou, A tuberculosis model with seasonality, *Bull. Math. Biol.*, **72** (2010), 931–952. https://doi.org/10.1007/s11538-009-9477-8
27. H. L. Smith, *Monotone Dynamical Systems: An Introduction to the Theory of Competitive and Cooperative Systems*, New York: American Mathematical Society, 1995.
28. H. L. Smith, P. Waltman, *The Theory of the Chemostat: Dynamics of Microbial Competition*, Cambridge: Cambridge University Press, 1995. https://doi.org/10.1017/CBO9780511530043
29. N. Bacaër, S. Guernaoui, The epidemic threshold of vector-borne diseases with seasonality, *J. Math. Biol.*, **53** (2006), 421–436. https://doi.org/10.1007/s00285-006-0015-0
30. N. Bacaër, S. Guernaoui, On the biological interpretation of a definition for the parameter $\mathcal{R}_0$ in periodic population models, *J. Math. Biol.*, **65** (2012), 601–621. https://doi.org/10.1007/s00285-011-0479-4
31. N. Bacaër, J. Ripoll, R. B. de La Parra, X. Bardina, S. Cuadrado, *Matemáticas y epidemias*, Paris: Cassini, 2021.
32. C. Mitchell, C. Kribs, A comparison of methods for calculating the basic reproductive number for periodic epidemic systems, *Bull. Math. Biol.*, **79** (2017), 1846–1869. https://doi.org/10.1007/s11538-017-0309-y
33. D. Posny, J. Wang, Computing the basic reproductive numbers for epidemiological models in nonhomogeneous environments, *Appl. Math. Comput.*, **242** (2014), 473–490. https://doi.org/10.1016/j.amc.2014.05.079
34. M. D. McKay, R. J. Beckman, W. J. Conover, Comparison of three methods for selecting values of input variables in the analysis of output from a computer code, *Technometrics*, **21** (1979), 239–245. https://doi.org/10.2307/1268522
35. F. Zhang, X. Q. Zhao, A periodic epidemic model in a patchy environment, *J. Math. Anal. Appl.*, **325** (2007), 496–516. https://doi.org/10.1016/j.jmaa.2006.01.085
36. X. Q. Zhao, *Dynamical Systems in Population Biology*, 2 Eds., Berlin: Springer, 2017. https://doi.org/10.1007/978-3-319-56433-3
37. *Measles (Rubeola)*, Centers for disease control and prevention, 2021. Available from: `https://www.cdc.gov/measles/about/index.html`.
38. *Measles*, World health organization, 2021. Available from: `https://www.who.int/news-room/fact-sheets/detail/measles`.
39. *Measles Monthly Bulletin*, World health organization, eastern mediterranean regional office (emro), 2021. Available from: `https://www.emro.who.int/vpi/publications/measles-monthly-bulletin.html`.
40. J. Huang, S. Ruan, X. Wu, X. Zhou, Seasonal transmission dynamics of measles in China, *Theory Biosci.*, **137** (2018), 185–195. https://doi.org/10.1007/s12064-018-0271-8

41. Y. Xue, X. Ruan, Y. Xiao, Modelling the periodic outbreak of measles in mainland China, *Math. Probl. Eng.*, **2020** (2020), 3631923. https://doi.org/10.1155/2020/3631923
42. J. Zhang, Z. Jin, G. Q. Sun, X. D. Sun, S. Ruan, Modeling seasonal rabies epidemics in China, *Bull. Math. Biol.*, **74** (2012), 1226–1251. https://doi.org/10.1007/s11538-012-9720-6
43. *Saudi Arabia-Health*, The world bank, 2021. Available from: `https://data.worldbank.org/country/saudi-arabia`.
44. *Pakistan-Health*, The world bank, 2021. Available from: `https://data.worldbank.org/country/pakistan`.
45. *Measles Monthly Bulletin*, World health organization, eastern mediterranean regional office (emro), 2021. Available from: `https://www.emro.who.int/vpi/publications/measles-monthly-bulletin.html`.
46. *Immunization, Vaccines and Biologicals, Measles*, World health organization (who). Available from: `https://www.who.int/teams/immunization-vaccines-and-biologicals/diseases/measles`.
47. *Pakistan-Immunizatio*, Gavi, 2021. Available from: `https://www.gavi.org/programmes-impact/country-hub/eastern-mediterranean/pakistan`.
48. J. Mossong, D. J. Nokes, W. J. Edmunds, M. J. Cox, S. Ratnam, C. P. Muller, Modeling the impact of subclinical measles transmission in vaccinated populations with waning immunity, *Amer. J. Epidemiol.*, **150** (1999), 1238–1249. https://doi.org/10.1093/oxfordjournals.aje.a009951
49. R. Anderson, B. Grenfell, Quantitative investigations of different vaccination policies for the control of congenital rubella syndrome (crs) in the united kingdom, *Epidemiol. Infect.*, **96** (1986), 305–333.
50. P. Van den Driessche, J. Watmough, Reproduction numbers and sub-threshold endemic equilibria for compartmental models of disease transmission, *Math. Biosci.*, **180** (2002), 29–48. https://doi.org/10.1016/S0025-5564(02)00108-6
51. L. Arriola, J. M. Hyman, Sensitivity analysis for uncertainty quantification in mathematical models, In: *Chowell, G., Hyman, J.M., Bettencourt, L.M.A., Castillo-Chavez, C. (eds) Mathematical and Statistical Estimation Approaches in Epidemiology*, Dordrecht: Springer, 2009, 195–247. https://doi.org/10.1007/978-90-481-2313-1_10
52. N. Bacaër, Approximation of the basic reproduction number $\mathcal{R}_0$ for vector-borne diseases with a periodic vector population, *Bull. Math. Biol.*, **69** (2007), 1067–1091. https://doi.org/10.1007/s11538-006-9166-9